

---

# L2R: Low-Rank and Lipschitz-Controlled Routing for Mixture-of-Experts

---

Minghao Yang Ren Togo Guang Li\* Takahiro Ogawa Miki Haseyama

Hokkaido University

Email: {yang, togo, guang, ogawa, mhaseyama}@lmd.ist.hokudai.ac.jp

## Abstract

Mixture-of-Experts (MoE) models scale neural networks by conditionally activating a small subset of experts, where the router plays a central role in determining expert specialization and overall model performance. However, many modern MoE systems still adopt linear routers in raw high-dimensional representation spaces, where representation mismatch, angular concentration, and scale-sensitive scoring can jointly undermine routing discriminability and stable expert specialization. In this work, we propose Low-rank & Lipschitz-controlled Routing (L2R), a unified routing framework that reshapes both the routing space and scoring geometry. L2R performs expert assignment in a shared low-rank latent routing space and introduces Saturated Inner-Product Scoring (SIPS) to explicitly control the Lipschitz behavior of routing functions, yielding smoother and more stable routing geometry. In addition, L2R incorporates a parameter-efficient multi-anchor routing mechanism to enhance expert expressiveness. Extensive experiments on an OLMoE-based language MoE model and a vision MoE setting on ImageNet demonstrate that L2R consistently improves routing geometry, expert discrimination, and overall model performance. Code will be released.

## 1 Introduction

Mixture-of-Experts (MoE) has emerged as a leading paradigm for scaling deep neural networks across a wide range of domains, including large language models (LLMs) [19, 8, 17, 31] and vision backbones [23, 4, 32]. By enabling conditional computation, MoE decouples model capacity from inference cost and is designed to realize meaningful expert specialization [3]. Central to achieving this objective is the router. As the mechanism that assigns tokens to experts under sparse and dynamic activation, the router effectively defines the functional topology of the model, governing how capacity is allocated and coordinated. Consequently, the quality of routing is a fundamental factor that determines the expressiveness, stability, and upper performance bound of MoE models [9].

Despite these advances, modern MoE routing still exhibits two practical limitations: 1) **Raw-space routing and high-dimensional concentration:** Routing is typically performed in raw, high-dimensional representation spaces that are optimized for representation learning rather than expert discrimination, resulting in a fundamental representation mismatch. Moreover, in high-dimensional spaces, similarities tend to concentrate [2], reducing effective separability among experts [5]. 2) **Scale-sensitive dot-product scoring:** Standard dot-product logits entangle directional alignment with feature scale, making routing highly sensitive to magnitude variations and encouraging norm-dominated competition among expert anchors, which introduces ambiguity in expert selection and weakens expert discrimination.

---

\*Correspondence to: Guang Li <guang@lmd.ist.hokudai.ac.jp>

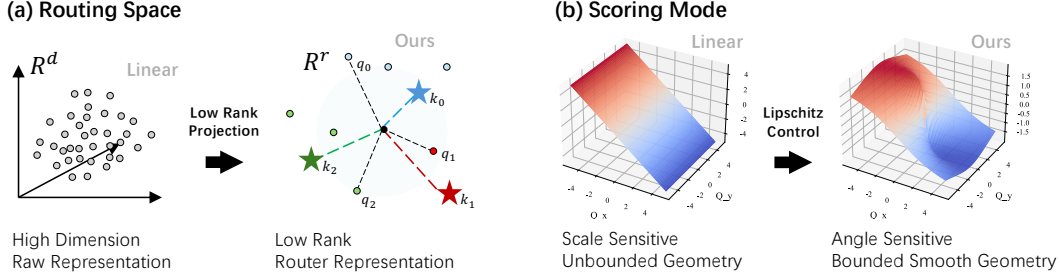


Figure 1: **Comparison between the linear router (left) and the proposed L2R framework (right).** (a) Routing space: Tokens are projected from high-dimensional raw representations into a low-rank routing space as  $q$ , where experts are represented by learnable anchors  $k$ . (b) Scoring mode: Compared to dot-product scoring, SIPS reshapes the score landscape into a bounded and smoother geometry, improving routing stability and expert discrimination.

To address these issues, we propose **Low-rank & Lipschitz-controlled Routing (L2R)**, a unified routing framework with three components: a low-rank routing space for representation decoupling, a Lipschitz-controlled scoring function for stable expert selection, and a parameter-efficient multi-anchor mechanism for enhanced expert expressiveness. **First**, instead of performing expert selection directly in the raw high-dimensional representation space, tokens are mapped into a shared low-rank routing space that produces routing-specific queries. Experts are represented by learnable anchors in this latent space, and routing is performed by matching queries to anchors. This design decouples routing from representation learning, compresses the search space for expert positioning, and alleviates geometric concentration in high-dimensional routing. **Second**, Saturated Inner-Product Scoring (SIPS) is introduced to bound the sensitivity of routing scores to representation scale and perturbations, thereby explicitly controlling the Lipschitz behavior of the routing function. By reshaping the score landscape into a smoother and more stable geometry, SIPS reduces routing ambiguity and promotes robust expert discrimination. **Finally**, we develop a parameter-efficient multi-anchor routing mechanism that associates each expert with multiple anchors, allowing a single expert to capture diverse semantic views without incurring prohibitive overhead.

We extensively evaluate the proposed L2R framework across diverse MoE settings to demonstrate its generality and effectiveness. Specifically, we conduct from-scratch training on large-scale language MoE models based on OLMoE [19] and evaluate vision MoE architectures on ImageNet using ViT backbones. Across both domains, our method consistently improves routing geometry, expert discrimination, and overall model performance, validating its effectiveness in both language and vision domains. We provide an expanded discussion of related work in Appendix A.

Our contributions are summarized as follows:

- We identify two practical limitations of linear MoE routing, namely routing in raw high-dimensional representation spaces and scale-sensitive dot-product scoring, which lead to routing ambiguity and insufficient expert specialization.
- We propose Low-rank & Lipschitz-controlled Routing (L2R), a unified routing framework that performs expert assignment in a low-rank latent routing space with Saturated Inner-Product Scoring (SIPS) and parameter-efficient multi-anchor routing, yielding smoother, more stable, and more expressive routing geometry.
- We validate L2R across both language and vision MoE settings, including OLMoE-based language models and vision backbones on ImageNet, consistently improving routing geometry, expert discrimination, and overall performance.

## 2 Methodology

In this section, we first introduce the standard formulation of MoE architecture and the commonly adopted linear routing mechanism. We then present the proposed L2R framework that reshapes both the routing space and the scoring geometry for stable and expressive expert specialization.

## 2.1 Preliminaries

**Mixture-of-Experts.** MoE models scale network capacity by replicating a sub-module, such as the feed-forward network (FFN) in a Transformer block, into a set of  $N$  parallel experts and activating only a sparse subset per input token [3]. Given an input representation  $\mathbf{x} \in \mathbb{R}^d$ , a router  $g(\cdot)$  first produces routing logits:

$$\mathbf{z} = g(\mathbf{x}) \in \mathbb{R}^N, \quad (1)$$

where each element  $z_i$  reflects the affinity between the token and expert  $E_i$ . The logits are then normalized via a softmax function with temperature  $\tau$  to obtain routing scores:

$$\mathbf{s} = \text{Softmax}(\mathbf{z}/\tau) \in \mathbb{R}^N. \quad (2)$$

A sparse gating mechanism subsequently selects the top- $k$  experts, and the final MoE output is computed as:

$$\mathbf{y} = \mathbf{x} + \sum_{i \in \mathcal{T}} s_i E_i(\mathbf{x}), \quad \mathcal{T} = \text{TopK}(\mathbf{s}, k), \quad (3)$$

where  $\mathcal{T}$  denotes the indices of the selected experts. The routing scores jointly determine expert activation and their relative contributions, thereby defining the effective mixture geometry and influencing expert specialization [9].

**Linear Router.** In most existing MoE architectures [19, 17, 31, 8], the router  $g(\cdot)$  is implemented as a dense linear transformation:

$$g(\mathbf{x}) = \mathbf{x} \mathbf{W}_g, \quad \mathbf{W}_g = [\mathbf{w}_1, \dots, \mathbf{w}_N] \in \mathbb{R}^{d \times N}, \quad (4)$$

where each column  $\mathbf{w}_i$  serves as the geometric anchor of expert  $E_i$ . The routing logit for expert  $E_i$  is computed as:

$$z_i = \mathbf{x}^\top \mathbf{w}_i, \quad (5)$$

which induces a partition of the high-dimensional representation space  $\mathbb{R}^d$  by linear decision hyperplanes defined by  $\{\mathbf{w}_i\}_{i=1}^N$ . This formulation performs expert assignment directly in raw backbone feature space using unbounded dot-product scoring, and thus inherits representation mismatch and scale-sensitive routing behaviors.

## 2.2 Low-Rank Routing

Linear routers perform expert assignment directly in the raw, high-dimensional backbone representation space. This design induces two structural limitations: 1) *representation mismatch* and 2) *high-dimensional concentration*, which fundamentally limit expert specialization.

**Representation Mismatch.** Backbone representations  $\mathbf{x}$  are primarily optimized for representation learning and downstream task prediction, rather than for expert discrimination. Consequently, the router is forced to operate in a *passive* feature space that is not explicitly shaped for separating tokens into expert-specific clusters. Especially in LLMs, semantic factors in such representations are often highly entangled due to superposition effects [10], and token distributions are not encouraged to organize into well-separated expert-aware regions. This representation mismatch makes it difficult for a linear router to induce stable and semantically coherent expert assignments.

**High-Dimensional Concentration.** Linear routing typically operates in a high-dimensional regime with  $d \gg N$  (e.g.,  $d = 4,096$  with  $N \leq 64$ ) [3]. In such spaces, angular similarities tend to concentrate [2], causing random or weakly structured vectors to become nearly orthogonal. Figure 2 compares the variance of pairwise token cosine similarities in the latent routing spaces of Linear, X-MoE [5], and L2R-SIPS on OL-MoE [19]. It provides direct empirical evidence of this phenomenon: backbone token representations for Linear routers exhibit near-zero variance in pairwise cosine similarity, indicating a highly concentrated angular geometry. As a result, routing logits across experts have poorly separated margins, leading to ambiguous

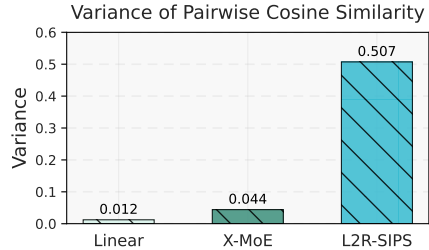


Figure 2: Layer-averaged variance of pairwise token cosine similarities in the routing space.

expert selection. Moreover, the large dimensionality of the routing space significantly enlarges the search space for expert anchors, making anchor optimization increasingly dependent on initialization and hindering effective expert positioning.

**Low-Rank Latent Routing Space.** To address the above limitations, we introduce a shared low-rank latent routing space that explicitly decouples routing from raw backbone geometry. Specifically, we parameterize routing through a shared projection:

$$\mathbf{q} = f(\mathbf{x}) = \mathbf{x}\mathbf{W}_q, \quad \mathbf{W}_q \in \mathbb{R}^{d \times r}, \quad r \ll d, \quad (6)$$

where  $\mathbf{q} \in \mathbb{R}^r$  denotes the routing-specific query representation. Each expert  $E_i$  is associated with a learnable anchor  $\mathbf{k}_i \in \mathbb{R}^r$  in this latent routing space, and routing logits are computed by matching  $\mathbf{q}$  with  $\{\mathbf{k}_i\}$ . This can be viewed as an attention-like operation, where  $\mathbf{q}$  serves as a routing query and  $\mathbf{k}_i$  as expert keys.

This formulation yields two immediate benefits: First, the shared projection  $\mathbf{W}_q$  explicitly learns a routing-oriented subspace, transforming backbone features into a space tailored for expert discrimination and mitigating raw-space representation mismatch. Second, routing in the compressed space  $\mathbb{R}^r$  substantially reduces geometric concentration and the anchor search space, enabling more stable anchor positioning and more discriminative expert selection. Figure 2 empirically supports this effect: with rank  $r=2$ , L2R-SIPS yields much higher pairwise-cosine variance than Linear and X-MoE, approaching the isotropic 2D reference value of 0.5 and indicating improved angular diversity.

### 2.3 Saturated Inner-Product Scoring (SIPS)

In this section, we analyze the limitations of standard dot-product scoring and introduce Saturated Inner-Product Scoring (SIPS), a bounded scoring geometry that balances the contributions of magnitude and angle for stable and expressive expert selection.

**Limitations of Dot-Product Scoring.** With low-rank routing (Section 2.2), a standard dot product typically computes logits as:

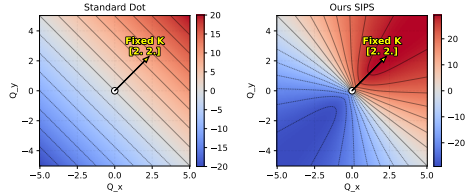
$$z_i = \mathbf{q}^\top \mathbf{k}_i = \|\mathbf{q}\| \|\mathbf{k}_i\| \cos \theta(\mathbf{q}, \mathbf{k}_i). \quad (7)$$

This coupling entangles *directional alignment* with *feature scale*. In practice, (i) token magnitudes  $\|\mathbf{q}\|$  can vary substantially (especially in LLMs, where certain token patterns yield unusually large activations), which scales all logits and effectively induces an input-dependent softmax temperature; and (ii) anchor norms  $\|\mathbf{k}_i\|$  modulate inter-expert logit gaps and can dominate the competition, since increasing  $\|\mathbf{k}_i\|$  often provides an easier route to raising scores than improving angular alignment. Together, these effects make routing scale-sensitive and encourage norm-dominated expert competition, introducing ambiguity in expert selection and weakening expert specialization.

**Geometric Visualization.** Figure 3 visualizes the logit landscape by fixing an expert anchor  $\mathbf{k}$  and sweeping query locations  $\mathbf{q}$  in a 2D routing plane. Under standard dot-product scoring (Figure 3a), level sets are nearly parallel lines, and the score grows linearly with  $\|\mathbf{q}\|$ , hence a large region shares similar scores, yielding weak angular discrimination and making expert selection sensitive to magnitude variations. This motivates a bounded scoring geometry that sharpens directional preference while controlling radial score growth, which we formalize next as SIPS.

**SIPS: Rebalancing Scale and Angle.** Cosine-style scoring like X-MoE [5] stabilizes routing by removing magnitude factors, but it also discards a potentially informative signal for adaptive gating. In contrast, SIPS rebalances *scale* and *angle*: it preserves magnitude information for adaptive scoring, while explicitly bounding its influence so that routing remains stable and controllable. Concretely, SIPS factorizes each logit into a bounded magnitude term and an angular term:

$$z_i = \phi(\|\mathbf{q}\|) \psi(\|\mathbf{k}_i\|) \cos \theta_i, \quad \cos \theta_i = \frac{\mathbf{q}^\top \mathbf{k}_i}{\|\mathbf{q}\| \|\mathbf{k}_i\|}, \quad (8)$$



(a) Dot Product Scoring (b) SIPS Scoring

Figure 3: **Score landscapes under fixed expert anchor.** Heatmaps visualize routing logits as a function of query location  $\mathbf{q} = (Q_x, Q_y)$  with a fixed anchor  $\mathbf{k} = [2, 2]$ .

where  $\phi(\cdot)$  and  $\psi(\cdot)$  are nonnegative scalar transforms. Compared to the previous methods, SIPS bounds the scale sensitivity in both tokens and anchors, while preserving the semantic role of angles and retaining a controlled contribution from magnitudes.

**Query Magnitude Transform**  $\phi(\|\mathbf{q}\|)$ . We bound query magnitudes through a *normalize-then-saturate* design. Normalization is applied first to stabilize the distribution of query norms: for vision models, we apply BatchNorm to the scalar norm  $\|\mathbf{q}\|$ , while for LLMs we apply RMSNorm [34] to the router input before the projection  $\mathbf{W}_q$ . We then define a bounded query magnitude transform:

$$\phi(\|\mathbf{q}\|) = \gamma \left( 1 + \beta \tanh(\widehat{\|\mathbf{q}\|}) \right), \quad (9)$$

where  $\widehat{\|\mathbf{q}\|}$  denotes the normalized query norm after the above normalization step. This yields a controllable interval:

$$\phi(\|\mathbf{q}\|) \in [\gamma(1 - \beta), \gamma(1 + \beta)]. \quad (10)$$

Here,  $\beta \in [0, 1]$  controls how much magnitude participates in expert selection ( $\beta = 0$  removes magnitude effects), and  $\gamma$  sets the overall logit scale (equivalently, it rescales logits and modulates the effective softmax temperature). This design mitigates excessively small logits for low-magnitude queries, while  $\tanh(\cdot)$  limits extreme magnitudes and prevents outliers from inducing overly sharp routing, hence improving routing stability. We provide an additional 3D score-landscape comparison across dot-product, cosine, and SIPS with varying  $\beta$  in Appendix D, which further illustrates the near-origin smoothness and controlled radial growth induced by query-magnitude saturation.

**Anchor Magnitude Transform**  $\psi(\|\mathbf{k}_i\|)$ . Anchor norms regulate inter-expert contribution and competitiveness under top- $k$  aggregation and hence should not be fully removed. However, to prevent norm-dominated competition, we compress anchor magnitudes around 1:

$$\psi(\|\mathbf{k}_i\|) = 1 + \frac{\|\mathbf{k}_i\| - 1}{p}. \quad (11)$$

With larger  $p$ , the marginal logit gain from increasing  $\|\mathbf{k}_i\|$  is dampened, encouraging experts to specialize primarily via angular alignment. We initialize anchors on the unit sphere ( $\|\mathbf{k}_i\| = 1$ ), so  $\psi(\|\mathbf{k}_i\|)$  is centered at 1 at initialization and deviations reflect learned competitiveness.

**Lipschitz-Controlled Score Geometry.** A key effect of SIPS is to *explicitly upper-bound the logit sensitivity* to scale variations, yielding a smoother and more controllable scoring geometry. Recall that in Equation (8),  $z_i = \phi(\|\mathbf{q}\|) \psi(\|\mathbf{k}_i\|) \cos \theta_i$ , the angular term satisfies  $\cos \theta_i \in [-1, 1]$  and is therefore intrinsically bounded. Consequently, scale-induced instability in dot-product scoring primarily arises from the magnitude factors  $\phi(\|\mathbf{q}\|)$  and  $\psi(\|\mathbf{k}_i\|)$ . SIPS addresses this by (i) bounding the query scale via  $\phi(\|\mathbf{q}\|)$  (Equation (9)) and (ii) compressing anchor norms around 1 via  $\psi(\|\mathbf{k}_i\|)$  (Equation (11)). These designs not only bound the attainable logit magnitude, but also bound the *slope* of  $z_i$  with respect to  $\|\mathbf{q}\|$  and  $\|\mathbf{k}_i\|$ , which directly translates into a smaller Lipschitz constant of the scoring map along the radial directions. Geometrically, this reshapes the fixed-anchor score field from an unbounded linear plane (Figure 3a) to a direction-selective landscape with controlled radial growth (Figure 3b), mitigating norm-driven ambiguity and improving the stability of expert selection. Formal gradient-sensitivity analysis and the resulting Lipschitz bounds for Equation (8) are provided in Appendix E.

## 2.4 Multi-Anchor Heads

While low-rank routing with SIPS provides a stable and discriminative scoring geometry, representing each expert with a single anchor can be restrictive when an expert needs to accommodate multiple semantic modes in the routing space. To increase routing expressiveness without introducing heavy routing overhead, we propose **multi-anchor heads**, which associate each expert with multiple anchors in the low-rank routing space.

**Multi-Anchor Parameterization.** For each expert  $E_i$ , we maintain  $H$  anchors  $\{\mathbf{k}_{i,h}\}_{h=1}^H$ , where  $\mathbf{k}_{i,h} \in \mathbb{R}^r$ . Given a routing query  $\mathbf{q}$ , we compute anchor-level logits under the SIPS geometry:

$$z_{i,h} = \phi(\|\mathbf{q}\|) \psi(\|\mathbf{k}_{i,h}\|) \cos \theta_{i,h}, \quad (12)$$

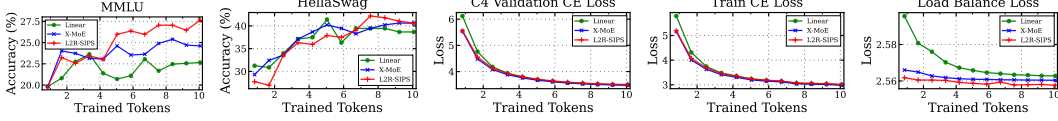


Figure 4: **OLMoE training dynamics.** Curves show MMLU and HellaSwag accuracies, C4 [21] validation cross-entropy (CE), training CE, and load-balance loss. L2R exhibits clear convergence over 10B tokens and consistently improves MMLU/HellaSwag.

where  $\cos \theta_{i,h} = \frac{\mathbf{q}^\top \mathbf{k}_{i,h}}{\|\mathbf{q}\| \|\mathbf{k}_{i,h}\|}$ . We then aggregate  $\{z_{i,h}\}_{h=1}^H$  into an expert-level logit  $z_i$  via log-sum-exp (LSE) pooling [16]:

$$z_i = \text{LSE}(\{z_{i,h}\}_{h=1}^H) = \log \sum_{h=1}^H \exp(z_{i,h}), \quad (13)$$

Compared to hard  $\max$  pooling, LSE provides a smooth approximation that yields more stable gradients while still emphasizing the best-matching anchor. Routing then proceeds as in Section 2.1 by applying softmax and top- $k$  selection on  $\{z_i\}_{i=1}^N$ . Geometrically, multi-anchor heads allow each expert to represent a union of directional regions in the routing space, improving coverage of multi-view semantics.

**Parameter Efficiency.** Multi-anchor heads only add low-dimensional anchors in  $\mathbb{R}^r$  and do not replicate the shared projection  $\mathbf{W}_q$ . As a result, the added parameters scale as  $O(NHr)$  and the extra computation is limited to low-rank inner products. A comprehensive efficiency analysis of L2R is provided in Appendix F.

**Initialization.** To align with the SIPS magnitude transforms, we initialize anchors on the unit sphere in  $\mathbb{R}^r$  (i.e.,  $\|\mathbf{k}_{i,h}\| = 1$ ) so that the initial competition is primarily driven by angular alignment, while norm-based competitiveness is learned gradually through  $\psi(\cdot)$ .

## 2.5 Optimization Objective

L2R is trained under the standard objective used in sparse MoE models, without introducing additional loss terms. The objective combines the task loss with auxiliary regularizers for routing stability and expert utilization:

$$\mathcal{L} = \mathcal{L}_{\text{task}} + \lambda_{\text{bal}} \mathcal{L}_{\text{bal}} + \lambda_z \mathcal{L}_z, \quad (14)$$

where  $\mathcal{L}_{\text{task}}$  is the task-specific training loss,  $\mathcal{L}_{\text{bal}}$  is the standard load-balancing loss [11] that encourages uniform expert usage, and  $\mathcal{L}_z$  is the router z-loss [35] for stabilizing routing logits during large-scale LLM training. The coefficients  $\lambda_{\text{bal}}$  and  $\lambda_z$  weight the auxiliary terms. Following OLMoE [19], we apply  $\mathcal{L}_z$  for LLM experiments and omit it for vision experiments. Formal definitions of  $\mathcal{L}_{\text{bal}}$  and  $\mathcal{L}_z$  are provided in Appendix G.

## 3 Experiments

This section evaluates L2R on both language and vision MoE systems. We first study OLMoE-based language MoE training [19] and report downstream benchmark performance under the OLMoE evaluation protocol. We then validate generality on a vision MoE system by training a ViT-S [27] backbone on ImageNet-1K [24].

### 3.1 LLM Experiments: OLMoE Pretraining

L2R is evaluated on OLMoE [19], an open MoE language model suite. The backbone and training recipe follow the OLMoE reference configuration with  $N=64$  experts and top- $k=8$  sparse activation. All models are trained *from scratch* for 10B tokens on a distribution-matched subset of the official OLMoE pretraining mixture; subset construction and domain statistics are reported in Appendix H. Unless stated otherwise, L2R uses rank  $r=2$  and  $H=16$  multi-anchor heads. For SIPS, we use  $\gamma=1$ ,  $\beta=1$  for the query transform (Equation 9) and  $p=4$  for the anchor transform (Equation 11). Full hyperparameters and implementation details are provided in Appendix I.1. All runs are conducted on an  $8 \times$  NVIDIA B200 setup.

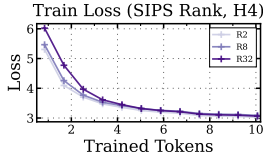
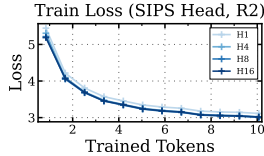
(a) Varying rank with  $H=4$ .(b) Varying heads with  $r=2$ .

Figure 5: **Training dynamics for ablations.** Both lower rank and more heads yield faster convergence.

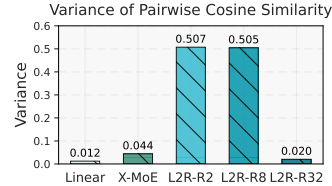


Figure 6: **Layer-averaged variance of pairwise token cosine similarities in the routing space.**

**Objective.** Training minimizes the standard cross entropy loss together with the auxiliary router regularizers adopted by OLMoE, including load-balancing loss and router z-loss (Section 2.5). Following OLMoE, the corresponding weights are set to  $\lambda_{\text{bal}}=0.01$  and  $\lambda_z=0.001$ .

**Compared Routers and L2R Variants.** The original OLMoE linear router is replaced by each of the compared routing designs. Baselines include the standard Linear router and a cosine scoring method X-MoE [5]. L2R is evaluated under different scoring geometries, including L2R (Dot), L2R (Cosine), and the proposed L2R (SIPS).

**Downstream Evaluation Protocol.** We follow the downstream evaluation protocol and reporting conventions of OLMoE [19]. Specifically, we track a fixed set of lightweight commonsense and knowledge benchmarks (e.g., MMLU [14], ARC-E [7], BoolQ [6], HellaSwag [33], PIQA [1], SciQ [28]) and report Overall as the average score across tasks. This suite is intentionally lightweight for 10B-token training to probe *early-stage* commonsense and knowledge capabilities while remaining stable and reproducible. Details of task selection and metrics are provided in Appendix K.

### 3.1.1 Main Results

**Training Dynamics.** Figure 4 summarizes training behavior over 10B tokens. All routers show smooth and monotonic loss reduction, confirming stable convergence under the OLMoE recipe. Throughout training, L2R consistently attains higher MMLU accuracy and remains competitive on HellaSwag. For both C4 [21] validation CE and training CE, L2R closely tracks the angle-sensitive baseline (X-MoE) and converges faster than the Linear router, supporting the benefit of stronger angular discrimination for optimization and generalization. Finally, in terms of load-balance loss, L2R achieves faster and lower convergence, indicating more balanced expert utilization and stable routing dynamics.

**Overall Performance.** Table 1 reports downstream evaluation results at 10B tokens. To isolate the effect of SIPS, we apply SIPS directly to the full-rank Linear router without low-rank projection or multi-anchor heads. Linear (SIPS) improves the overall score from 40.5 to 42.1, showing that SIPS alone can provide a clear gain over dot-product scoring. L2R with the proposed low-rank routing and SIPS further achieves the best overall score (43.4) and ranks first or second on most benchmarks. Notably, L2R yields a substantial gain on MMLU, improving from 22.7 (Linear) and 24.6 (X-MoE) to 27.6, indicating stronger early-stage knowledge recall and reasoning on lightweight probes. We also observe an exception on ARC-E, where L2R trails the Linear router; consistent with the head ablation in Table 3, the ARC-E drop becomes more pronounced as the number of heads increases, suggesting that the multi-anchor specialization pattern may require longer training to benefit ARC-style multiple-choice questions fully.

Table 1: Overall performance at 10B tokens.

| Method            | MMLU        | ARC-E       | BoolQ       | HSwag       | PIQA        | SciQ        | Overall     |
|-------------------|-------------|-------------|-------------|-------------|-------------|-------------|-------------|
| Linear            | 22.7        | <b>47.7</b> | 60.0        | 38.7        | 61.1        | 66.8        | 40.5        |
| Linear (SIPS)     | 24.2        | 46.1        | <b>61.7</b> | <b>42.6</b> | <u>63.5</u> | 68.4        | <u>42.1</u> |
| X-MoE             | 24.6        | 46.9        | 60.0        | 40.6        | <b>64.5</b> | 68.8        | <u>42.1</u> |
| L2R (Dot)         | 24.4        | <u>43.4</u> | 59.2        | 39.5        | 60.5        | 64.8        | 40.6        |
| L2R (Cosine)      | <u>24.9</u> | 42.2        | <u>61.1</u> | <u>42.2</u> | 60.0        | <b>72.7</b> | 42.0        |
| <b>L2R (SIPS)</b> | <b>27.6</b> | 43.8        | <b>61.7</b> | 40.6        | 62.3        | <u>71.5</u> | <b>43.4</b> |

*Note:* Best results are in **bold**, and second-best results are underlined.

**Angle Discrimination vs. Scale Domination.** The results reveal a consistent split between (i) *angle-sensitive* routing and (ii) *unconstrained dot-product* routing. Angle-sensitive designs (X-MoE, L2R (Cosine), and L2R (SIPS)) substantially outperform Linear and L2R (Dot) in overall quality, and

also exhibit faster cross-entropy reduction during training (Figure 4), underscoring the importance of angular discrimination for reliable routing. Meanwhile, pure cosine scoring eliminates magnitude cues, whereas SIPS retains them with bounded influence. This controlled rebalancing yields stronger overall performance over X-MoE and L2R (Cosine), supporting the role of *controlled* magnitude in expressive yet stable expert aggregation.

### 3.1.2 Ablations Study

**Ablation on Routing Rank  $r$ .** Table 2 varies the routing rank with  $H=4$ . We find that ultra-low rank is sufficient:  $r=2$  achieves the best overall score, and larger ranks bring no consistent gains. Increasing  $r$  can reduce angular diversity (lower pairwise cosine-similarity variance in Figure 6), yielding a more concentrated routing geometry and less discriminative expert assignment. Consistently, Figure 5a shows slower training convergence for higher ranks. A similar trend is observed in our vision MoE study (Section 3.2).

Table 2: Ablation on routing rank  $r$  with  $H = 4$ .

| Rank | MMLU        | ARC-E       | BoolQ       | HSwag       | PIQA        | SciQ        | Overall     |
|------|-------------|-------------|-------------|-------------|-------------|-------------|-------------|
| 2    | 25.2        | <b>45.7</b> | 62.1        | <b>39.5</b> | 61.1        | 69.1        | <b>42.0</b> |
| 8    | 23.2        | 43.4        | <b>62.3</b> | 38.3        | <b>63.1</b> | 68.8        | 41.0        |
| 32   | <b>25.6</b> | 43.4        | 59.4        | 39.1        | 61.1        | <b>71.9</b> | 41.9        |

**Ablation on Multi-Anchor Heads  $H$ .** Table 3 varies the head count with  $r=2$ . Increasing  $H$  improves overall performance up to a moderate range, with the best result obtained at  $H=16$ ; however, further increasing  $H$  to 64 does not yield additional gains. This suggests

Table 3: Ablation on multi-anchor heads  $H$  with rank  $r=2$ .

| $H$ | Router Params  | MMLU        | ARC-E       | BoolQ       | HSwag       | PIQA        | SciQ        | Overall     |
|-----|----------------|-------------|-------------|-------------|-------------|-------------|-------------|-------------|
| 1   | 100.4K (4.79%) | 25.5        | <b>46.9</b> | 60.0        | 37.5        | 60.5        | 69.9        | 41.9        |
| 4   | 106.5K (5.08%) | 25.2        | 45.7        | 62.1        | 39.5        | 61.1        | 69.1        | 42.0        |
| 8   | 114.7K (5.47%) | 25.2        | 45.3        | 60.2        | 39.8        | <b>64.3</b> | 68.4        | 42.1        |
| 16  | 131.1K (6.25%) | <b>27.6</b> | 43.8        | 61.7        | <b>40.6</b> | 62.3        | <b>71.5</b> | <b>43.4</b> |
| 64  | 196.6K (9.38%) | 26.9        | <b>46.9</b> | <b>62.1</b> | 40.2        | 62.1        | 68.8        | 42.8        |

*Note:* Router parameters are reported over all MoE layers, with percentages relative to the Linear router.

a practical head-selection guideline: a moderate number of heads, such as  $H=8$  or  $H=16$ , provides a favorable trade-off between multi-view routing capacity and anchor redundancy. These results support the effectiveness of the multi-anchor routing pattern, which enriches routing flexibility in the low-rank space without incurring prohibitive router overhead.

### 3.1.3 Routing Geometry and Expert Usage Visualizations

#### Routing-Space Geometry.

Figure 7 contrasts token geometry in the raw backbone space  $\mathbf{x}$  and the projected routing space  $\mathbf{q}$ . Under Linear routing (Figure 7a), tokens concentrate in an anisotropic and “narrow” region, consistent with the severe angular concentration quantified in Figure 6. In contrast, L2R learns a routing-oriented low-rank space where token directions are markedly more separable and form structured regions when stratified by top-1 expert assignments (Figure 7c). Tracing these same tokens back to the raw  $\mathbf{x}$  space reveals wide dispersion (Figure 7b), which is consistent with a multi-anchor specialization pattern that each expert covers multiple semantic modes instead of a single compact cluster in  $\mathbf{x}$ .

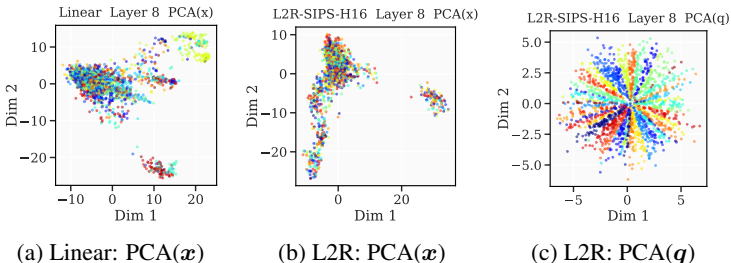


Figure 7: **Representation-space visualization.** PCA projections of token representations in the raw backbone space ( $\mathbf{x}$ ) and the low-rank routing space ( $\mathbf{q}$ ). Points are colored by the top-1 routed expert.

**Near-Origin Stability with SIPS.** Both the raw and projected routing spaces contain low-magnitude tokens around the origin, where routing is inherently noise-sensitive (cosine-style scoring can be particularly brittle to small angular perturbations). SIPS stabilizes this regime by imposing a bounded and smooth magnitude response, avoiding vanishing scores for low-norm queries, thereby improving stability without discarding magnitude information. Further diagnostics and ablations on  $\phi(\cdot)$  are provided in Appendix D.

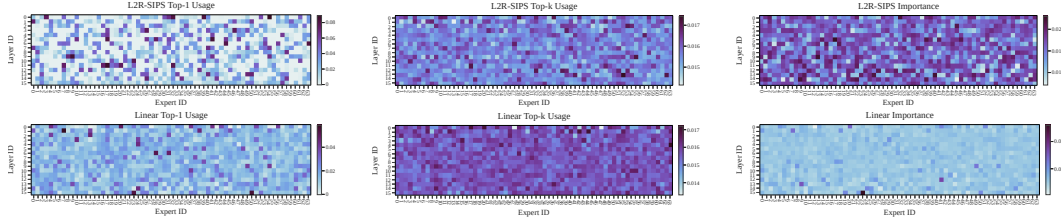


Figure 8: **Expert-usage patterns.** Each row is a Transformer layer, and each column is an expert. From left to right: top-1 frequency, top- $k$  frequency, and importance-based routing weights.

**Expert Usage and Cooperation.** Figure 8 summarizes routing patterns across layers. Compared to Linear routing, L2R yields a sharper and more structured top-1 map, indicating clearer expert specialization, while maintaining broadly distributed top- $k$  usage, reflecting sustained cooperation under sparse activation. Importantly, regions with high top-1 frequency do not consistently align with peaks in the top- $k$  and importance maps, suggesting that L2R avoids single-expert domination and instead modulates multi-expert contributions via SIPS-controlled magnitude. We further provide quantitative routing diagnostics in Appendix B, including margin-based expert-discrimination metrics and perturbation-based robustness measurements.

### 3.2 Experiments with ViT on ImageNet

We further evaluate L2R on a vision MoE system by training a ViT-S [27] backbone on ImageNet-1K [24] *from scratch* for 300 epochs. We follow a standard ViT-S recipe with batch size 512 and apply MoE to the last 4 Transformer blocks. Unless stated otherwise, we use  $N=16$  experts with top- $k=2$  sparse activation, and train with only the load-balancing auxiliary loss ( $\lambda_{\text{bal}}=0.01$ ). For L2R, we set rank  $r=2$  and multi-anchor heads  $H=4$ , and reuse the same SIPS hyperparameters as in the LLM setting ( $\gamma=1$ ,  $\beta=1$ ,  $p=4$ ). All runs are conducted on  $4 \times$  A100 GPUs. Detailed configurations are summarized in Appendix I.2.

Table 4: Top-1 and Top-5 accuracy on ImageNet-1K with ViT-S backbone.

| Method            | Top-1 (%) $\uparrow$ | Top-5 (%) $\uparrow$ |
|-------------------|----------------------|----------------------|
| Linear            | 74.12                | 90.38                |
| X-MoE             | 74.07                | 90.23                |
| L2R (Dot)         | 74.96                | 91.23                |
| L2R (Cosine)      | 75.32                | 91.36                |
| <b>L2R (SIPS)</b> | <b>76.58</b>         | <b>91.50</b>         |

**Performance on ImageNet.** Table 4 reports ImageNet results. L2R achieves the best performance, confirming that L2R with the proposed SIPS transfers effectively to vision MoE training. Notably, X-MoE [5] slightly underperforms the Linear router in this setting, whereas L2R variants yield consistent gains, suggesting that improving routing geometry is beneficial beyond the language domain. Additional ablations on routing rank and multi-anchor heads are provided in Appendix C.

## 4 Conclusion

We introduced **Low-rank & Lipschitz-controlled Routing (L2R)**, a routing framework that improves MoE specialization by jointly redesigning the routing space and scoring geometry. L2R replaces high-dimensional linear routing with a shared low-rank latent space, adopts Saturated Inner-Product Scoring (SIPS) to bound magnitude sensitivity while preserving controlled magnitude for adaptive expert weighting, and extends expressiveness with lightweight multi-anchor heads. Experiments on OLMoE pretraining and ViT-based ImageNet training show consistent gains on most benchmarks, faster convergence, and balanced expert usage, indicating that L2R provides a practical and stable routing recipe across both language and vision MoE systems. We discuss limitations and future directions in Appendix L, and broader impacts in Appendix M.

## References

- [1] Yonatan Bisk, Rowan Zellers, Jianfeng Gao, Yejin Choi, et al. Piqa: Reasoning about physical commonsense in natural language. In *Proc. AAAI*, volume 34, pages 7432–7439, 2020.
- [2] Tony Cai, Jianqing Fan, and Tiefeng Jiang. Distributions of angles in random packing on spheres. *J. Mach. Learn. Res.*, 14(1):1837–1864, 2013.
- [3] Weilin Cai, Juyong Jiang, Fan Wang, Jing Tang, Sunghun Kim, and Jiayi Huang. A survey on mixture of experts in large language models. *IEEE Trans. Knowl. Data Eng.*, 2025.
- [4] Zitian Chen, Yikang Shen, Mingyu Ding, Zhenfang Chen, Hengshuang Zhao, Erik G Learned-Miller, and Chuang Gan. Mod-squad: Designing mixtures of experts as modular multi-task learners. In *Proc. CVPR*, pages 11828–11837, 2023.
- [5] Zewen Chi, Li Dong, Shaohan Huang, Damai Dai, Shuming Ma, Barun Patra, Saksham Singhal, Payal Bajaj, Xia Song, Xian-Ling Mao, et al. On the representation collapse of sparse mixture of experts. In *Proc. NeurIPS*, pages 34600–34613, 2022.
- [6] Christopher Clark, Kenton Lee, Ming-Wei Chang, Tom Kwiatkowski, Michael Collins, and Kristina Toutanova. Boolq: Exploring the surprising difficulty of natural yes/no questions. *arXiv preprint arXiv:1905.10044*, 2019.
- [7] Peter Clark, Isaac Cowhey, Oren Etzioni, Tushar Khot, Ashish Sabharwal, Carissa Schoenick, and Oyvind Tafjord. Think you have solved question answering? try arc, the ai2 reasoning challenge. *arXiv preprint arXiv:1803.05457*, 2018.
- [8] Damai Dai, Chengqi Deng, Chenggang Zhao, RX Xu, Huazuo Gao, Deli Chen, Jiashi Li, Wangding Zeng, Xingkai Yu, Yu Wu, et al. Deepseekmoe: Towards ultimate expert specialization in mixture-of-experts language models. *arXiv preprint arXiv:2401.06066*, 2024.
- [9] Nishanth Dikkala, Nikhil Ghosh, Raghu Meka, Rina Panigrahy, Nikhil Vyas, and Xin Wang. On the benefits of learning to route in mixture-of-experts models. In *Proc. EMNLP*, pages 9376–9396, 2023.
- [10] Nelson Elhage, Tristan Hume, Catherine Olsson, Nicholas Schiefer, Tom Henighan, Shauna Kravec, Zac Hatfield-Dodds, Robert Lasenby, Dawn Drain, Carol Chen, et al. Toy models of superposition. *arXiv preprint arXiv:2209.10652*, 2022.
- [11] William Fedus, Barret Zoph, and Noam Shazeer. Switch transformers: Scaling to trillion parameter models with simple and efficient sparsity. *J. Mach. Learn. Res.*, 23(120):1–39, 2022.
- [12] Trevor Gale, Deepak Narayanan, Cliff Young, and Matei Zaharia. Megablocks: Efficient sparse training with mixture-of-experts. In *Proc. MLSys*, volume 5, pages 288–304, 2023.
- [13] Yuling Gu, Oyvind Tafjord, Bailey Kuehl, Dany Haddad, Jesse Dodge, and Hannaneh Hajishirzi. OLMES: A standard for language model evaluations. In *Proc. NAACL*, pages 5005–5033, 2025.
- [14] Dan Hendrycks, Collin Burns, Steven Basart, Andy Zou, Mantas Mazeika, Dawn Song, and Jacob Steinhardt. Measuring massive multitask language understanding. In *Proc. ICLR*, 2021.
- [15] Changho Hwang, Wei Cui, Yifan Xiong, Ziyue Yang, Ze Liu, Han Hu, Zilong Wang, Rafael Salas, Jithin Jose, Prabhat Ram, et al. Tutel: Adaptive mixture-of-experts at scale. In *Proc. MLSys*, volume 5, pages 269–287, 2023.
- [16] Yangqing Jia, Chang Huang, and Trevor Darrell. Beyond spatial pyramids: Receptive field learning for pooled image features. In *Proc. CVPR*, pages 3370–3377, 2012.
- [17] Albert Q Jiang, Alexandre Sablayrolles, Antoine Roux, Arthur Mensch, Blanche Savary, Chris Bamford, Devendra Singh Chaplot, Diego de las Casas, Emma Bou Hanna, Florian Bressand, et al. Mixtral of experts. *arXiv preprint arXiv:2401.04088*, 2024.
- [18] Dmitry Lepikhin, HyoukJoong Lee, Yuanzhong Xu, Dehao Chen, Orhan Firat, Yanping Huang, Maxim Krikun, Noam Shazeer, and Zhifeng Chen. Gshard: Scaling giant models with conditional computation and automatic sharding. *arXiv preprint arXiv:2006.16668*, 2020.

- [19] Niklas Muennighoff, Luca Soldaini, Dirk Groeneveld, Kyle Lo, Jacob Morrison, Sewon Min, Weijia Shi, Pete Walsh, Oyvind Tafjord, Nathan Lambert, et al. OLMoE: Open mixture-of-experts language models. In *Proc. ICLR*, 2025.
- [20] Huy Nguyen, Pedram Akbarian, Trang Pham, Trang Nguyen, Shujian Zhang, and Nhat Ho. Statistical advantages of perturbing cosine router in mixture of experts. In *Proc. ICLR*, 2025.
- [21] Colin Raffel, Noam Shazeer, Adam Roberts, Katherine Lee, Sharan Narang, Michael Matena, Yanqi Zhou, Wei Li, and Peter J Liu. Exploring the limits of transfer learning with a unified text-to-text transformer. *J. Mach. Learn. Res.*, 21(140):1–67, 2020.
- [22] Junfeng Ran, Guangxiang Zhao, Yuhan Wu, Dawei Zhu, Longyun Wu, Yikai Zhao, Tong Yang, Lin Sun, Xiangzheng Zhang, and Sujian Li. Router upcycling: Leveraging mixture-of-routers in mixture-of-experts upcycling. *arXiv preprint arXiv:2509.00679*, 2025.
- [23] Carlos Riquelme, Joan Puigcerver, Basil Mustafa, Maxim Neumann, Rodolphe Jenatton, André Susano Pinto, Daniel Keysers, and Neil Houlsby. Scaling vision with sparse mixture of experts. In *Proc. NeurIPS*, pages 8583–8595, 2021.
- [24] Olga Russakovsky, Jia Deng, Hao Su, Jonathan Krause, Sanjeev Satheesh, Sean Ma, Zhiheng Huang, Andrej Karpathy, Aditya Khosla, Michael Bernstein, et al. Imagenet large scale visual recognition challenge. *Int. J. Comput. Vis.*, 115(3):211–252, 2015.
- [25] Keisuke Sakaguchi, Ronan Le Bras, Chandra Bhagavatula, and Yejin Choi. Winogrande: An adversarial winograd schema challenge at scale. In *Proc. AAAI*, volume 34, pages 8732–8740, 2020.
- [26] Noam Shazeer, Azalia Mirhoseini, Krzysztof Maziarz, Andy Davis, Quoc Le, Geoffrey Hinton, and Jeff Dean. Outrageously large neural networks: The sparsely-gated mixture-of-experts layer. *arXiv preprint arXiv:1701.06538*, 2017.
- [27] Hugo Touvron, Matthieu Cord, Matthijs Douze, Francisco Massa, Alexandre Sablayrolles, and Hervé Jégou. Training data-efficient image transformers & distillation through attention. In *Proc. ICML*, pages 10347–10357, 2021.
- [28] Johannes Welbl, Nelson F Liu, and Matt Gardner. Crowdsourcing multiple choice science questions. *arXiv preprint arXiv:1707.06209*, 2017.
- [29] Shaohua Wu, Jiangang Luo, Xi Chen, Lingjun Li, Xudong Zhao, Tong Yu, Chao Wang, Yue Wang, Fei Wang, Weixu Qiao, et al. Yuan 2.0-m32: Mixture of experts with attention router. *arXiv preprint arXiv:2405.17976*, 2024.
- [30] Xun Wu, Shaohan Huang, Wenhui Wang, Shuming Ma, Li Dong, and Furu Wei. Multi-head mixture-of-experts. In *Proc. NeurIPS*, pages 94073–94096, 2024.
- [31] An Yang, Baosong Yang, Binyuan Hui, et al. Qwen2 technical report. *arXiv preprint arXiv:2407.10671*, 2024.
- [32] Minghao Yang, Ren Togo, Guang Li, Takahiro Ogawa, and Miki Haseyama. Adaptive shared experts with LoRA-based mixture of experts for multi-task learning. *arXiv preprint arXiv:2510.00570*, 2025.
- [33] Rowan Zellers, Ari Holtzman, Yonatan Bisk, Ali Farhadi, and Yejin Choi. Hellaswag: Can a machine really finish your sentence? *arXiv preprint arXiv:1905.07830*, 2019.
- [34] Biao Zhang and Rico Sennrich. Root mean square layer normalization. In *Proc. NeurIPS*, 2019.
- [35] Barret Zoph, Irwan Bello, Sameer Kumar, Nan Du, Yanping Huang, Jeff Dean, Noam Shazeer, and William Fedus. St-moe: Designing stable and transferable sparse expert models. *arXiv preprint arXiv:2202.08906*, 2022.

## Impact Statement

This work proposes a routing framework for Mixture-of-Experts models that improves routing stability, expert specialization, and efficiency through low-rank representations and Lipschitz-controlled scoring. By enabling more reliable sparse activation, the method can support more stable training and effective use of model capacity in large-scale language and vision models. The contribution is primarily technical and focuses on internal optimization of Mixture-of-Experts architectures, without introducing new application-level capabilities beyond existing scalable model designs; any broader societal impacts depend on downstream deployment choices.

## A Related Work

**Router Design in Sparse MoE.** Most modern sparse MoE systems still rely on raw-space linear routing, where expert logits are produced by a single linear projection in the backbone representation space, e.g., in OLMoE [19], Mixtral [17], Qwen2-MoE [31], and DeepSeek-MoE [8], as well as vision MoE variants such as V-MoE [23], Mod-Squad [4], and ASE [32]. Recent studies revisit router design from multiple angles: improving routing expressiveness (e.g., Router Upcycling [22] and attention-based routing in Yuan 2.0-M32 [29]), and improving stability and utilization via auxiliary objectives and routing variants [26, 18, 11]. Despite these advances, the routing score is still typically produced by *linear scoring in a high-dimensional space*, which leaves the scoring geometry sensitive to scale and high-dimensional concentration.

**Geometry-Aware Latent-Space Routing.** Another line of work performs routing in a *latent space* and adopts angle-aware similarities [5, 20, 30]. X-MoE [5] projects representations to a lower-dimensional space and uses cosine scoring to alleviate collapse in high-dimensional gating. Different from prior works, our study emphasizes two structural limitations that jointly weaken discriminability under raw-space routing: representation mismatch and angular concentration. We further observe that common rank heuristics (e.g., scaling rank with the number of experts) can still yield an angle-concentrated routing geometry in practice, motivating an ultra-low yet *consistent* rank across settings. Within this latent-space routing paradigm, L2R introduces *SIPS*, a Lipschitz-controlled scoring geometry that retains magnitude cues while explicitly bounding their effective influence (instead of discarding magnitude as cosine scoring), and improves expressiveness via lightweight multi-anchor heads.

## B Quantitative Diagnostics of Routing Behavior

### B.1 Quantitative Metrics for Expert Discrimination

To complement PCA visualizations and routing heatmaps, we introduce two quantitative metrics for expert discrimination. *Mean Routing Margin* measures the average logit gap between the Top-1 expert and the Top-2 expert, while *Low-Margin Rate* measures the proportion of tokens whose routing margin is smaller than 0.2. A larger margin indicates clearer separation between the selected expert and its strongest competitor, whereas a lower low-margin rate indicates fewer tokens near the routing decision boundary. As shown in Table 5, X-MoE and L2R (Dot)-H1 exhibit small margins and high low-margin rates, suggesting weak expert separation. In contrast, L2R with SIPS substantially increases the routing margin and reduces the low-margin rate, providing direct quantitative evidence that SIPS leads to more separated and decisive routing decisions.

Table 5: Direct expert-discrimination metrics.

| Model          | Mean Margin $\uparrow$ | Low-Margin Rate $\downarrow$ |
|----------------|------------------------|------------------------------|
| X-MoE          | 0.0712                 | 0.9424                       |
| L2R (Dot)-H1   | 0.0105                 | 0.9989                       |
| L2R (SIPS)-H1  | <b>0.1806</b>          | 0.7036                       |
| L2R (SIPS)-H16 | 0.1718                 | <b>0.6701</b>                |

### B.2 Routing Robustness under Perturbations

To directly validate the stability benefit of SIPS, we apply Gaussian noise with  $\sigma = 0.02$  to router inputs and measure two perturbation-based routing robustness metrics: Stability of the top-1 routed expert and Top- $k$  Overlap (Jaccard similarity of the selected top-8 expert set).

As shown in Table 6, these results provide direct empirical support for the stability claim. Comparing Linear to Linear (SIPS) shows that SIPS improves routing robustness even in the full-rank representation space, indicating that the scoring function itself contributes to stable expert selection. More importantly, low-rank routing with unconstrained dot-product scoring, i.e., L2R (Dot)-H1, becomes highly fragile, with stability dropping to 0.6734 and top- $k$  overlap dropping to 0.8311. In contrast, replacing the unbounded dot product with SIPS largely restores robustness, achieving 0.9847 stability and 0.9915 top- $k$  overlap for L2R (SIPS)-H1. These results clarify the component roles: the low-rank projection reshapes the routing geometry, whereas SIPS makes the resulting low-rank routing stable in practice. We therefore emphasize bounded-domain control of radial sensitivity, rather than unconstrained global smoothness.

Table 6: Routing robustness under Gaussian perturbations.

| Model         | Stability $\uparrow$ | Top- $k$ Overlap $\uparrow$ |
|---------------|----------------------|-----------------------------|
| Linear        | 0.9744               | 0.9679                      |
| Linear (SIPS) | <b>0.9853</b>        | <b>0.9805</b>               |
| X-MoE         | 0.9566               | 0.9683                      |
| L2R (Dot)-H1  | 0.6734               | 0.8311                      |
| L2R (SIPS)-H1 | <b>0.9847</b>        | <b>0.9915</b>               |

*Note:* Higher values indicate more stable routing decisions.

## C Ablation Study for ImageNet

We provide ImageNet-1K ablation studies to analyze the effects of the routing rank  $r$  and the number of multi-anchor heads  $H$  in vision MoE training.

Table 7: Ablation on routing rank  $r$  with  $H = 4$  on ImageNet-1K.

| Rank | Top-1 (%) $\uparrow$ | Top-5 (%) $\uparrow$ |
|------|----------------------|----------------------|
| 2    | <b>76.58</b>         | <b>91.50</b>         |
| 8    | 75.44                | 90.95                |
| 32   | 74.90                | 90.12                |

**Ablation on Routing Rank  $r$ .** Table 7 varies the routing rank with fixed  $H=4$ . Consistent with the LLM results, we find that ultra-low rank is sufficient:  $r=2$  performs best, while increasing rank to 8 or 32 degrades accuracy. This supports the same geometric conclusion that enlarging the routing space can reintroduce concentration effects and reduce angular separability, weakening expert discrimination even in vision settings.

Table 8: Ablation on multi-anchor heads  $H$  with rank  $r=2$  on ImageNet-1K.

| Head | Top-1 (%) $\uparrow$ | Top-5 (%) $\uparrow$ |
|------|----------------------|----------------------|
| 1    | 75.47                | 91.31                |
| 4    | <b>76.58</b>         | 91.50                |
| 8    | 76.22                | <b>91.79</b>         |
| 16   | 75.20                | 91.00                |

**Ablation on Multi-Anchor Heads  $H$ .** Table 8 varies the head count with fixed  $r=2$ . We observe the strongest performance at a moderate head count around  $H=4$ ; larger  $H$  does not yield consistent gains and can slightly degrade accuracy. This suggests that, for ImageNet-1K with relatively limited MoE depth applied to only the last 4 layers, excessive anchor multiplicity may over-fragment routing regions and introduce overfitting, whereas a small number of anchors provides sufficient multi-mode coverage.

## D Additional Geometry of Query-Magnitude Saturation

Figure 9 provides a complementary 3D visualization of routing score landscapes under a fixed anchor, highlighting how different scoring rules respond to variations in query magnitude. We fix  $\mathbf{k} = [-2, 0]$  and sweep  $\mathbf{q} = (Q_x, Q_y)$  over a 2D routing plane, plotting the resulting logit value  $z(\mathbf{q}, \mathbf{k})$ .

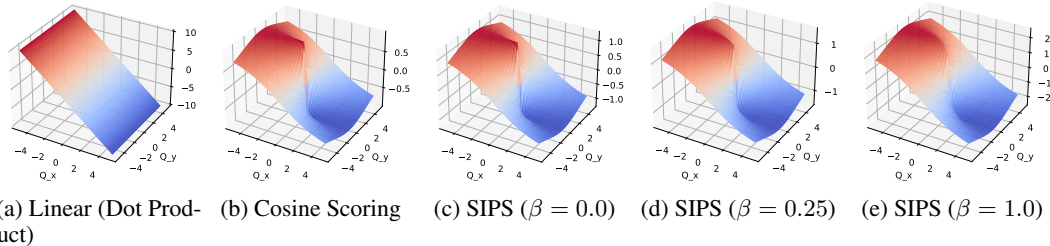


Figure 9: **Effect of query-magnitude saturation strength ( $\beta$ ) under a fixed anchor.** We fix the expert anchor at  $\mathbf{k} = [-2, 0]$  and visualize routing logits over query locations  $\mathbf{q} = (Q_x, Q_y)$  in a 2D routing plane (rank  $r = 2$ ). Dot-product scoring produces an unbounded, nearly half-space-like field dominated by radial growth (a), whereas cosine scoring removes magnitude effects entirely (b). SIPS interpolates between these extremes by preserving magnitude as a bounded confidence signal: increasing  $\beta$  enlarges the effective dynamic range of the bounded magnitude term while maintaining controlled radial growth (c–e).

**Dot-Product Scoring.** As shown in Figure 9a, standard dot-product scoring yields an (approximately) half-space-like field whose value grows linearly with  $\|\mathbf{q}\|$  along the radial direction. This implies that scale variations can dominate the score landscape, creating large regions with weak angular contrast while simultaneously allowing extreme magnitudes to induce overly sharp routing.

**Cosine Scoring.** Cosine scoring (Figure 9b) eliminates magnitude effects by normalizing both  $\mathbf{q}$  and  $\mathbf{k}$ , thereby improving global scale stability. However, the normalization introduces a sharp behavior around  $\|\mathbf{q}\| \approx 0$ , where small perturbations of low-norm queries can cause disproportionately large changes in direction (and thus in  $\cos \theta$ ). Since low-norm queries are also more susceptible to noise, this “origin sharpness” can translate into unstable and noisy expert selection.

**SIPS Scoring.** SIPS introduces a bounded query-magnitude transform  $\phi(\|\mathbf{q}\|) = \gamma(1 + \beta \tanh(\widehat{\|\mathbf{q}\|}))$  and thus treats magnitude as a *bounded confidence* factor rather than an unbounded amplifier. When  $\beta = 0$  (Figure 9c),  $\phi(\|\mathbf{q}\|)$  becomes a constant, and the logit reduces to a cosine-like form up to a global rescaling, removing magnitude participation. As  $\beta$  increases (Figure 9d and 9e), magnitude information is gradually reintroduced, but its influence remains strictly bounded; importantly, the score landscape becomes noticeably **smoother around the origin** while preserving **clear directional selectivity**. This yields a controlled radial growth together with improved near-origin smoothness, which empirically corresponds to more stable routing dynamics and less noise-sensitive expert selection.

**Takeaway.** Overall, Figure 9 illustrates that SIPS is not merely “bounded” in value, but also reshapes the score geometry into a smoother, angle-sensitive landscape. The saturation strength  $\beta$  governs how strongly query magnitude participates in routing: smaller  $\beta$  emphasizes angular discrimination with minimal scale effects, while larger  $\beta$  leverages magnitude as a bounded confidence signal without recovering the unbounded norm dominance of dot-product scoring.

## E Gradient Sensitivity and Lipschitz Bounds of SIPS

We analyze the gradient sensitivity of the SIPS logit in Equation (8) and derive Lipschitz bounds under mild domain assumptions that match practical routing implementations.

**Setup.** For a single expert, define  $\rho = \|\mathbf{q}\|$ ,  $\kappa = \|\mathbf{k}\|$ ,  $\mathbf{u} = \mathbf{q}/\rho$ ,  $\mathbf{v} = \mathbf{k}/\kappa$ , and  $c = \mathbf{u}^\top \mathbf{v} = \cos \theta \in [-1, 1]$ . The SIPS logit can be written as:

$$z(\mathbf{q}, \mathbf{k}) = \phi(\rho) \psi(\kappa) c. \quad (15)$$

As in practice, we assume numerical stabilization by enforcing:

$$\rho \geq \varepsilon_q, \quad \kappa \geq \varepsilon_k, \quad (16)$$

for small  $\varepsilon_q, \varepsilon_k > 0$ .

**Cosine gradient bound.** Using  $\mathbf{u} = \mathbf{q}/\rho$  and treating  $\mathbf{v}$  as fixed, the cosine alignment satisfies:

$$\nabla_{\mathbf{q}}c = \frac{1}{\rho}(\mathbf{I} - \mathbf{u}\mathbf{u}^\top)\mathbf{v}, \quad \|\nabla_{\mathbf{q}}c\| \leq \frac{1}{\rho}. \quad (17)$$

Symmetrically:

$$\nabla_{\mathbf{k}}c = \frac{1}{\kappa}(\mathbf{I} - \mathbf{v}\mathbf{v}^\top)\mathbf{u}, \quad \|\nabla_{\mathbf{k}}c\| \leq \frac{1}{\kappa}. \quad (18)$$

**Gradient sensitivity of SIPS.** Differentiating Equation (15) yields:

$$\nabla_{\mathbf{q}}z = \psi(\kappa)\left(\phi'(\rho)c\mathbf{u} + \phi(\rho)\nabla_{\mathbf{q}}c\right), \quad (19)$$

$$\nabla_{\mathbf{k}}z = \phi(\rho)\left(\psi'(\kappa)c\mathbf{v} + \psi(\kappa)\nabla_{\mathbf{k}}c\right). \quad (20)$$

Using  $|c| \leq 1$  and Equations (17)–(18), we obtain:

$$\|\nabla_{\mathbf{q}}z\| \leq \psi(\kappa)\left(|\phi'(\rho)| + \frac{\phi(\rho)}{\rho}\right), \quad (21)$$

$$\|\nabla_{\mathbf{k}}z\| \leq \phi(\rho)\left(|\psi'(\kappa)| + \frac{\psi(\kappa)}{\kappa}\right). \quad (22)$$

**Lipschitz bounds on a practical domain.** A global Lipschitz constant requires bounded magnitudes. We therefore analyze  $z$  on the domain:

$$\mathcal{D} = \{\mathbf{q}, \mathbf{k} : \rho \in [\varepsilon_q, \rho_{\max}], \kappa \in [\varepsilon_k, \kappa_{\max}]\}, \quad (23)$$

where  $\rho_{\max}$  is induced by normalization and  $\kappa_{\max}$  is induced by weight decay or explicit norm control. Assume on  $\mathcal{D}$  that  $\phi(\rho) \leq \phi_{\max}$ ,  $|\phi'(\rho)| \leq L_\phi$ , and  $\psi(\kappa) \leq \psi_{\max}$ ,  $|\psi'(\kappa)| \leq L_\psi$ . Then by Equations (21)–(22),  $z$  is Lipschitz in  $\mathbf{q}$  and  $\mathbf{k}$  with:

$$\text{Lip}_{\mathbf{q}}(z) \leq \psi_{\max}\left(L_\phi + \frac{\phi_{\max}}{\varepsilon_q}\right), \quad (24)$$

$$\text{Lip}_{\mathbf{k}}(z) \leq \phi_{\max}\left(L_\psi + \frac{\psi_{\max}}{\varepsilon_k}\right). \quad (25)$$

A joint Lipschitz bound with respect to  $(\mathbf{q}, \mathbf{k})$  follows by combining the two gradient bounds.

**Instantiation for our transforms.** For the query transform  $\phi(\rho) = \gamma(1 + \beta \tanh(\widehat{\rho}))$ , we have:

$$\phi_{\max} = \gamma(1 + \beta), \quad \left|\frac{d\phi}{d\rho}\right| \leq \gamma\beta. \quad (26)$$

Thus  $L_\phi \leq \gamma\beta L_{\text{norm}}$  if the scalar normalization map  $\rho \mapsto \widehat{\rho}$  is  $L_{\text{norm}}$ -Lipschitz on  $\mathcal{D}$ . For the anchor transform  $\psi(\kappa) = 1 + (\kappa - 1)/p$ , we have:

$$L_\psi = \frac{1}{p}, \quad \psi_{\max} = 1 + \frac{\kappa_{\max} - 1}{p} \text{ on } \mathcal{D}. \quad (27)$$

**Contrast to dot-product scoring.** For  $z_{\text{dot}}(\mathbf{q}, \mathbf{k}) = \mathbf{q}^\top \mathbf{k}$ , the gradients are  $\nabla_{\mathbf{q}}z_{\text{dot}} = \mathbf{k}$  and  $\nabla_{\mathbf{k}}z_{\text{dot}} = \mathbf{q}$ , so sensitivity grows linearly with  $\|\mathbf{k}\|$  and  $\|\mathbf{q}\|$ . In contrast, SIPS bounds the radial sensitivity via bounded/contractive magnitude transforms, and therefore yields an explicit mechanism to control the Lipschitz behavior of the scoring map.

## F Complexity and Efficiency

We analyze the routing overhead of L2R and compare it to the standard linear router. Let  $d$  be the backbone hidden dimension,  $N$  the number of experts,  $r$  the routing rank ( $r \ll d$ ),  $k$  the top- $k$  sparsity, and  $H$  the number of anchors per expert in multi-anchor heads.

**Baseline: Linear Routing.** A standard linear router computes logits by  $z = \mathbf{x}\mathbf{W}_g$  with  $\mathbf{W}_g \in \mathbb{R}^{d \times N}$  as Equation (4). The routing parameter count is:

$$P_{\text{lin}} = dN, \quad (28)$$

and the per-token routing cost is dominated by the matrix-vector product:

$$C_{\text{lin}} \approx O(dN). \quad (29)$$

**L2R Routing.** L2R replaces the high-dimensional projection by (i) a shared low-rank projection  $\mathbf{W}_q \in \mathbb{R}^{d \times r}$  and (ii) expert anchors  $\{\mathbf{k}_{i,h}\}$  in  $\mathbb{R}^r$ . With multi-anchor heads, L2R maintains  $NH$  anchors.

**Parameters.** The routing parameters consist of  $\mathbf{W}_q$  and anchors:

$$P_{\text{L2R}} = dr + NHr. \quad (30)$$

Thus, the parameter reduction over linear routing is:

$$\frac{P_{\text{L2R}}}{P_{\text{lin}}} = \frac{dr + NHr}{dN} = \frac{r}{N} + \frac{Hr}{d}. \quad (31)$$

In typical MoE settings where  $d \gg r$  and  $N$  is moderate-to-large, the router overhead is substantially reduced, and the multi-anchor term remains small because it scales only with  $r$ .

**Computation.** L2R first computes  $\mathbf{q} = \mathbf{x}\mathbf{W}_q$  with cost  $O(dr)$ , then evaluates anchor logits by low-rank inner products with cost  $O(NHr)$ :

$$C_{\text{L2R}} \approx O(dr + NHr). \quad (32)$$

SIPS adds only lightweight scalar transforms on norms and does not change the asymptotic complexity. Multi-anchor pooling aggregates  $H$  logits per expert as Equation (13), which is  $O(NH)$  and negligible compared to  $O(NHr)$  when  $r \geq 2$ .

**Measured Router Parameters on OLMoE.** Table 9 reports router parameter counts under different rank-head combinations on OLMoE (16 MoE layers,  $d=2048$ ,  $N=64$ ). Each entry shows the total router parameters aggregated over all MoE layers, followed by the percentage relative to the Linear router (2.097M parameters). Across all tested configurations, router parameters remain negligible compared to the full model size ( $\sim 6.92\text{B}$ ), and multi-anchor heads incur only a minor additional cost.

Table 9: **Router parameters under different rank  $r$  and head  $H$  settings on OLMoE.** Each cell reports total router params over all MoE layers, with the percentage relative to the Linear router (2.097M) in parentheses.

| Rank $r$ \ Heads $H$ | 1                 | 2                 | 4                 | 8                 | 16                |
|----------------------|-------------------|-------------------|-------------------|-------------------|-------------------|
| 2                    | 100.352K (4.79%)  | 102.400K (4.88%)  | 106.496K (5.08%)  | 114.688K (5.47%)  | 131.072K (6.25%)  |
| 4                    | 167.936K (8.01%)  | 172.032K (8.20%)  | 180.224K (8.59%)  | 196.608K (9.38%)  | 229.376K (10.94%) |
| 8                    | 303.104K (14.46%) | 311.296K (14.84%) | 327.680K (15.62%) | 360.448K (17.19%) | 425.984K (20.32%) |
| 16                   | 573.440K (27.34%) | 589.824K (28.12%) | 622.592K (29.69%) | 688.128K (32.81%) | 819.200K (39.07%) |
| 32                   | 1.114M (53.11%)   | 1.147M (54.68%)   | 1.212M (57.81%)   | 1.343M (64.06%)   | 1.606M (76.59%)   |

**Discussion: FLOPs vs. Wall-Clock Time.** Although  $O(dr + NHr)$  can be significantly smaller than  $O(dN)$ , practical end-to-end speedups are not guaranteed. Routing is often not the dominant cost of MoE blocks, and the L2R router introduces additional element-wise operations (normalization, tanh, and pooling) that may be less hardware-efficient than a single dense GEMM.

To quantify practical inference cost, we further measure wall-clock latency and throughput on  $8 \times \text{B200}$  GPUs with batch size 1, averaged over 5 samples.

As shown in Table 10, L2R introduces only a small prefill overhead relative to Linear. For example, L2R (SIPS)-H16 is close to Linear in prefill latency (182.36 ms vs. 180.78 ms), while decode latency increases by about 3.3 ms/step. This is consistent with our complexity analysis: L2R is parameter-efficient, but theoretical savings do not automatically translate into end-to-end wall-clock gains without further kernel- and system-level optimization.

Table 10: Inference overhead on OLMoE.

| Model          | Prefill Latency (ms) ↓ | Prefill Tok/s ↑ | Decode Latency (ms/step) ↓ | Decode Tok/s ↑ |
|----------------|------------------------|-----------------|----------------------------|----------------|
| Linear         | 180.78                 | 22657.39        | 43.79                      | 22.84          |
| L2R (Dot)-H1   | 181.94                 | 22512.97        | 46.29                      | 21.60          |
| L2R (SIPS)-H1  | 187.08                 | 21894.31        | 47.06                      | 21.25          |
| L2R (SIPS)-H16 | 182.36                 | 22461.40        | 47.12                      | 21.22          |

## G Optimization Objective Details

We train L2R under the standard optimization objective adopted by prior sparse MoE models, without introducing additional loss terms. Specifically, the objective consists of the task loss, a load-balancing loss to encourage uniform expert utilization, and the router z-loss [35] used in OLMoE [19] to stabilize gating logits in large-scale language model training.

**Load-Balancing Loss.** Following prior MoE work, we employ a load-balancing loss to prevent expert under-utilization and collapse. Let  $s_{t,i}$  denote the routing probability assigned to expert  $i$  for token  $t$ , and let  $\mathbb{I}[i \in \mathcal{T}_t]$  indicate whether expert  $i$  is selected in the top- $k$  routing set for token  $t$ . Over a batch of  $T$  tokens, we define the average routing probability and empirical expert usage as:

$$\bar{s}_i = \frac{1}{T} \sum_{t=1}^T s_{t,i}, \quad f_i = \frac{1}{T} \sum_{t=1}^T \mathbb{I}[i \in \mathcal{T}_t]. \quad (33)$$

The load-balancing loss is then given by:

$$\mathcal{L}_{\text{bal}} = N \sum_{i=1}^N \bar{s}_i f_i, \quad (34)$$

which encourages alignment between routing probabilities and actual expert assignments.

**Z-Loss.** Following OLMoE [19], we additionally employ the router z-loss for large-scale language model training to regularize the magnitude of pre-softmax routing logits. Let  $z_t \in \mathbb{R}^N$  denote the routing logits for token  $t$ . The z-loss is defined as:

$$\mathcal{L}_z = \frac{1}{T} \sum_{t=1}^T \left( \log \sum_{i=1}^N \exp(z_{t,i}) \right)^2, \quad (35)$$

which discourages excessively large logits and improves training stability. We apply this term only in LLM training, and omit it for vision and multi-task learning experiments.

**Overall Objective.** The final optimization objective is:

$$\mathcal{L} = \mathcal{L}_{\text{task}} + \lambda_{\text{bal}} \mathcal{L}_{\text{bal}} + \lambda_z \mathcal{L}_z, \quad (36)$$

where  $\lambda_{\text{bal}}$  and  $\lambda_z$  control the relative weights of the auxiliary losses.

## H Experiments with OLMoE: Data Preparation

**Source dataset.** We use the official OLMoE pretraining mixture `allenai/OLMoE-mix-0924`, which contains approximately 4.07T tokens spanning six domains. To accelerate experimentation while preserving the training distribution, we construct a smaller, distribution-matched subset by sampling complete shards from each domain in proportion to its scale in the full mix.

**Distribution-matched shard sampling.** Let  $\mathcal{D} = \{d\}$  denote the set of domains and let  $S_d$  be the number of shards in domain  $d$ . Given a target budget of  $T$  tokens (e.g.,  $T = 200\text{B}$ ), we randomly sample a fixed number of shards from each domain using a fixed seed (seed=2025), such that the resulting token mass closely matches the original mixture proportions. Concretely, we sample shards without replacement within each domain, and keep the domain-wise sampling ratios aligned with the full dataset scale. Table 11 reports the resulting domain composition for the 200B subset used in our main OLMoE experiments.

Table 11: **Distribution-matched 200B subset of allenai/OLMoE-mix-0924.** We randomly sample complete shards per domain with a fixed seed (2025) to obtain a  $\approx 200\text{B}$ -token subset while preserving the domain mixture ratios of the full dataset.

| Domain          | Total shards | Selected shards | Approx. tokens (B) | Token share (%) |
|-----------------|--------------|-----------------|--------------------|-----------------|
| dclm            | 1970         | 97              | 190.06             | 94.01           |
| starcoder       | 863          | 43              | 5.03               | 2.49            |
| pes2o           | 26           | 1               | 2.20               | 1.09            |
| open-web-math   | 26           | 1               | 0.49               | 0.24            |
| algebraic-stack | 16           | 1               | 0.79               | 0.39            |
| wiki            | 2            | 1               | 1.84               | 0.91            |
| <b>Total</b>    | 2903         | 144             | 200.41             | 100.00          |

**Multiple subset sizes.** Using the same procedure, we also generate additional subsets at smaller scales (10B/50B/100B tokens) for fast ablations and debugging. All subsets are constructed by the same distribution-matched shard sampling strategy to ensure comparability across scales.

## I Training Configuration Details

### I.1 Training Configuration for OLMoE Experiments

This appendix reports the core training hyperparameters for OLMoE experiments in Table 12. To isolate routing effects, we follow the original OLMoE [19] settings and keep the backbone architecture, optimization recipe, and MoE auxiliary losses fixed across all router variants, modifying only router-specific components (e.g., projection rank, scoring, or head design) when applicable.

Table 12: **Key hyperparameters for OLMoE training.**

| Item                   | Value           | Item                          | Value              | Item                 | Value       |
|------------------------|-----------------|-------------------------------|--------------------|----------------------|-------------|
| $d_{\text{model}}$     | 2,048           | Max sequence length           | 4,096              | Experts $N$          | 64          |
| Transformer layers $L$ | 16              | Vocabulary size               | 50,280             | Top- $k$             | 8           |
| Attention heads        | 16              | Load-balance weight           | 0.01               | Droptout routing     | on          |
| $n_{\text{heads}}$     |                 | $\lambda_{\text{bal}}$        |                    |                      |             |
| MLP ratio              | 1               | Z-loss weight $\lambda_z$     | 0.001              | Type                 | AdamW       |
| Activation             | SwiGLU          | Learning rate                 | $4 \times 10^{-4}$ | $(\beta_1, \beta_2)$ | (0.9, 0.95) |
| Norm                   | RMSNorm         | $\epsilon$                    | $10^{-8}$          | Weight decay         | 0.1         |
| Warmup tokens          | $3 \times 10^8$ | Total tokens $t_{\text{max}}$ | $10^{10}$          | Decay                | cosine      |
| $t_{\text{warmup}}$    |                 |                               |                    |                      |             |
| Global batch size      | 1024            | Microbatch size               | 1                  | Distributed training | DDP         |

**Implementation Details.** All models are trained from scratch on the 10B-token in-distribution dataset described in Appendix H. We follow the standard OLMoE recipe with a Transformer backbone of  $d_{\text{model}} = 2048$ ,  $N = 64$  experts per MoE block, and top- $k = 8$  sparse activation. Optimization is performed using AdamW with cosine learning-rate decay, and all experiments are trained with Distributed Data Parallel (DDP) for scalability and stability. All runs are conducted on an  $8 \times \text{NVIDIA B200}$  (Blackwell) setup.

The original OLMoE implementation relies on Megablocks [12] for MoE kernel acceleration. However, Megablocks currently does not support Blackwell sm\_100 image configuration, which limits its compatibility on B200. To ensure correct execution and efficient expert dispatch, we replace the Megablocks MoE module with Tutel [15], which offers architecture-agnostic kernels and stable performance under modern GPU backends. This change affects only the MoE dispatch backend and does not alter the routing logic or model formulation, ensuring fair and controlled comparisons across routing variants. For full reproducibility, we will release the complete configuration files and training scripts with the codebase.

### I.2 Training Configuration for ViT Experiments

This appendix reports the core training hyperparameters for ViT ImageNet experiments in Table 13. To isolate routing effects, we keep the backbone architecture, augmentation recipe, and optimization

Table 13: Key hyperparameters for ViT-S ImageNet-1K training.

| Item                               | Value    | Item                 | Value              | Item                 | Value     |
|------------------------------------|----------|----------------------|--------------------|----------------------|-----------|
| Model                              | ViT-S/16 | Image size           | 224                | #Classes             | 1000      |
| ViT depth                          | 12       | Epochs               | 300                | Batch size (per GPU) | 128       |
| Optimizer                          | AdamW    | Learning rate        | $5 \times 10^{-4}$ | Min LR               | $10^{-6}$ |
| Weight decay                       | 0.05     | Warmup epochs        | 5                  | Grad clip            | 1.0       |
| RandAugment                        | on       | Random erasing prob. | 0.25               | Label smoothing      | 0.1       |
| Mixup                              | 0.8      | CutMix               | 1.0                |                      |           |
| Experts $N$                        | 16       | Top- $k$             | 2                  | MoE last- $n$ blocks | 4         |
| Aux. weight $\lambda_{\text{bal}}$ | 0.01     | Learnable $\tau$     | false              |                      |           |

settings fixed across router variants, and only modify router-specific components (e.g., router type, rank, scoring mode, or head design) when applicable.

## J Full Experimental Results for OLMoE Experiments

Table 14: Downstream performance at the checkpoint closest to 10B total tokens (%). We report all four MMLU groups and their mean (MMLU), five additional tasks, and the overall mean (Overall) across nine tasks. Best results are in bold, and second-best results are underlined.

| Method       | H  | Rank | Hum         | Other       | SocSci      | STEM        | MMLU        | ARC-E       | BoolQ       | HSwag       | PIQA        | SciQ        | Overall     |
|--------------|----|------|-------------|-------------|-------------|-------------|-------------|-------------|-------------|-------------|-------------|-------------|-------------|
| X-MoE        | -  | 32   | 23.4        | <b>30.1</b> | 25.8        | 19.1        | 24.6        | <u>46.9</u> | 60.0        | <u>40.6</u> | <b>64.5</b> | 68.8        | <u>42.1</u> |
| Linear       | -  | -    | 22.3        | 21.5        | 27.0        | 19.9        | 22.7        | <b>47.7</b> | 60.0        | 38.7        | 61.1        | 66.8        | 40.5        |
| L2R (Cosine) | -  | 2    | 22.3        | 27.3        | 30.1        | 19.9        | 24.9        | 42.2        | 61.1        | <b>42.2</b> | 60.0        | <b>72.7</b> | 42.0        |
| L2R (Dot)    | -  | 2    | <u>25.4</u> | <u>30.9</u> | 21.1        | <u>20.3</u> | 24.4        | 43.4        | 59.2        | 39.5        | 60.5        | 64.8        | 40.6        |
| L2R (SIPS)   | 16 | 2    | <b>28.9</b> | 25.8        | <b>34.8</b> | <b>21.1</b> | <b>27.6</b> | 43.8        | 61.7        | <u>40.6</u> | 62.3        | 71.5        | <b>43.4</b> |
| L2R (SIPS)   | 8  | 2    | 22.7        | 26.2        | <u>32.0</u> | 19.9        | 25.2        | 45.3        | 60.2        | 39.8        | <u>64.3</u> | 68.4        | <u>42.1</u> |
| L2R (SIPS)   | 4  | 2    | 24.2        | 28.1        | 29.3        | 19.1        | 25.2        | 45.7        | <u>62.1</u> | 39.5        | 61.1        | 69.1        | 42.0        |
| L2R (SIPS)   | 4  | 32   | 23.8        | 27.7        | 31.2        | 19.5        | <u>25.6</u> | 43.4        | 59.4        | 39.1        | 61.1        | 71.9        | 41.9        |
| L2R (SIPS)   | 1  | 2    | 22.7        | 27.0        | 31.2        | <b>21.1</b> | 25.5        | <u>46.9</u> | 60.0        | 37.5        | 60.5        | 69.9        | 41.9        |
| L2R (SIPS)   | 4  | 8    | 25.0        | 23.8        | 24.6        | 19.5        | 23.2        | 43.4        | <b>62.3</b> | 38.3        | 63.1        | 68.8        | 41.0        |

## K Downstream Evaluation Protocol

We follow the downstream evaluation protocol used by OLMoE [19] and OLMES [13] for reporting model quality. Specifically, we evaluate a fixed set of commonsense and knowledge benchmarks at checkpoints along training and report the average score (**Overall**) across all included tasks. All evaluations are performed using the same prompt format and normalization conventions as in the OLMoE/OLMES setup.

### K.1 Tasks and Metrics

Table 15 summarizes the tasks and evaluation settings used in this work. We report task accuracy for all benchmarks. For MMLU [14], we follow the standard multiple-choice formulation and report both the mean MMLU score and the four group scores (Humanities, Social Sciences, STEM, Other) in Appendix J.

### K.2 Early-Stage Evaluation

Our language MoE models are trained from scratch up to **10B tokens**. At this early pretraining stage, some downstream benchmarks commonly reported in OLMoE/OLMES (e.g., WinoGrande [25] and ARC-Challenge [7]) tend to exhibit high variance and unstable ranking across checkpoints, because the model has not yet formed sufficiently robust linguistic and commonsense representations. Including such tasks at 10B tokens can introduce noise that obscures routing-induced differences. Therefore, we focus on a compact set of tasks (Table 15) that are more stable and informative in the 10B-token regime, and we report an overall mean across these tasks for comparability.

Table 15: **Summary of downstream evaluation.** We adopt the OLMoE/OLMES evaluation conventions. CF = completion/cloze (generative) formulation; MCF = multiple-choice formulation; Norm indicates the answer normalization used by the evaluator. ARC-E refers to ARC-Easy.

| Dataset        | Format       | Norm | Metric   |
|----------------|--------------|------|----------|
| MMLU [14]      | MCF (5-shot) | char | Accuracy |
| ARC-E [7]      | CF (0-shot)  | none | Accuracy |
| BoolQ [6]      | CF (0-shot)  | none | Accuracy |
| HellaSwag [33] | CF (0-shot)  | char | Accuracy |
| PIQA [1]       | CF (0-shot)  | char | Accuracy |
| SciQ [28]      | CF (0-shot)  | none | Accuracy |

### K.3 Benchmark Descriptions

We evaluate downstream quality using a compact suite of widely-used benchmarks that probe complementary capabilities (knowledge, reading comprehension, commonsense reasoning, and scientific QA). Below, we briefly describe each benchmark and the associated evaluation interface used in our pipeline.

**MMLU.** Massive Multitask Language Understanding (MMLU) is a broad knowledge benchmark covering dozens of subjects spanning the humanities, social sciences, STEM, and other domains. Each example is a multiple-choice question with four candidate options. We evaluate MMLU in the standard multiple-choice formulation (MCF) and report accuracy. In addition to the overall MMLU mean, we optionally report the four group means (Hum, SocSci, STEM, Other) to diagnose capability skew across domains.

**ARC-E.** ARC-Easy (ARC-E) is a grade-school science QA benchmark focusing on relatively accessible science and commonsense questions. Each example provides a question and multiple candidate answers. Following prior work, we score candidates using conditional likelihood and select the best option, reporting accuracy. ARC-E tends to provide an early signal of improving general reasoning and basic scientific knowledge during pretraining.

**BoolQ.** BoolQ is a yes/no question answering benchmark grounded in short passages. Given a passage and a question, the model predicts a binary label (yes or no). We evaluate with accuracy. BoolQ emphasizes reading comprehension and entailment-style reasoning, and it is typically less sensitive to prompt formatting than many open-ended generation tasks.

**HellaSwag.** HellaSwag is a commonsense inference benchmark framed as sentence completion. Given a context, the model must choose the most plausible continuation from multiple candidates. We compute a score for each candidate continuation via conditional likelihood and report accuracy. HellaSwag probes grounded commonsense and causal/temporal plausibility, and is commonly used to reflect progress in event-level reasoning.

**PIQA.** PIQA tests physical commonsense reasoning for everyday situations. Each example describes a goal (e.g., how to accomplish a household task) and provides two candidate solutions; the model must select the more plausible one. We evaluate via candidate scoring and report accuracy. PIQA complements HellaSwag by focusing specifically on physical affordances and action feasibility.

**SciQ.** SciQ is a science QA dataset consisting of multiple-choice questions derived from science exams and accompanying explanations. We evaluate in the standard candidate-scoring setup and report accuracy. SciQ provides an additional view of science knowledge that is often more structured than ARC-style questions.

## L Limitation and Future Work

A limitation of our study is that the language experiments focus on an early-stage OLMoE-based pretraining regime. This setting is chosen to enable controlled router comparisons under identical

data mixture, architecture, optimization schedule, and auxiliary routing losses. While the results consistently show improved routing geometry and downstream performance at 10B tokens, further scaling to longer pretraining budgets and larger MoE configurations remains an important direction for future work.

In addition, this work primarily evaluates L2R under representative language and vision MoE settings. Future work may further investigate how the optimal routing rank and number of anchors vary with model size, expert count, and training duration. Extending L2R to additional architectures, downstream adaptation scenarios, and more diverse deployment settings would also help better understand its generality and practical impact.

## **M Impact Statement**

This work proposes a routing framework for Mixture-of-Experts models that improves routing stability, expert specialization, and efficiency through low-rank representations and Lipschitz-controlled scoring. By enabling more reliable sparse activation, the method can support more stable training and effective use of model capacity in large-scale language and vision models. The contribution is primarily technical and focuses on internal optimization of Mixture-of-Experts architectures, without introducing new application-level capabilities beyond existing scalable model designs; any broader societal impacts depend on downstream deployment choices.

## N Visualizations for OLMoE

### N.1 Visualizations for OLMoE Training Results

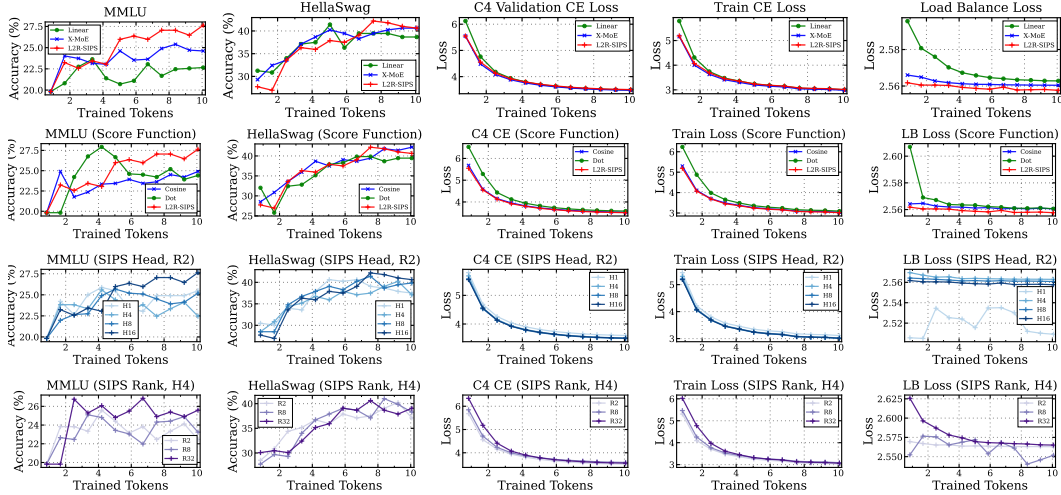


Figure 10: **Visualizations of OLMoE training dynamics.** The panels report MMLU accuracy, HellaSwag accuracy, C4 validation cross-entropy (CE), training CE, and load-balance loss across router variants. From top to bottom, we compare alternative methods, scoring modes, and ablations over head and rank settings. The x-axis denotes the number of trained tokens.

### N.2 Routing Geometry Visualizations in OLMoE

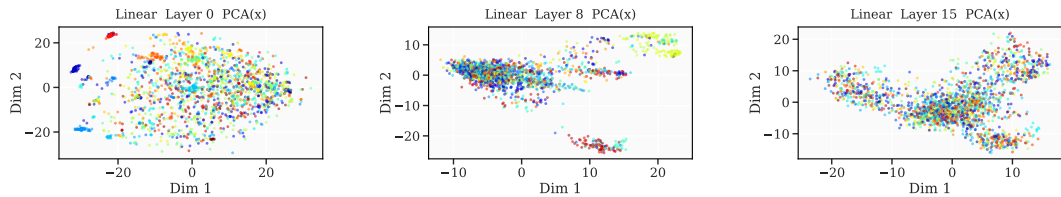


Figure 11: **Linear-router baselines.** PCA scatter plots in backbone representation space ( $x$ -space) for the same layers as Figure 12. Tokens are colored by the top-1 expert assignment under a linear router. These baselines help contrast expert separation in raw representations against our L2R latent routing space.

This section provides qualitative visualizations of routing geometry in the OLMoE setting. For selected MoE FFN layers (early-0; middle-8; late-15), we project token representations to two dimensions using PCA. Each point corresponds to a token representation and is colored by its top-1 routed expert. We visualize (i) the backbone representation space ( $x$ -space) and (ii) the routing latent space ( $q$ -space) produced by our low-rank projection. These plots support two observations: (1) routing in raw high-dimensional representations can lead to ambiguous expert separation, while (2) our routing latent space yields clearer cluster structure aligned with expert assignment, making the routing geometry more interpretable. We additionally report linear-router and X-MoE baselines for direct comparison.

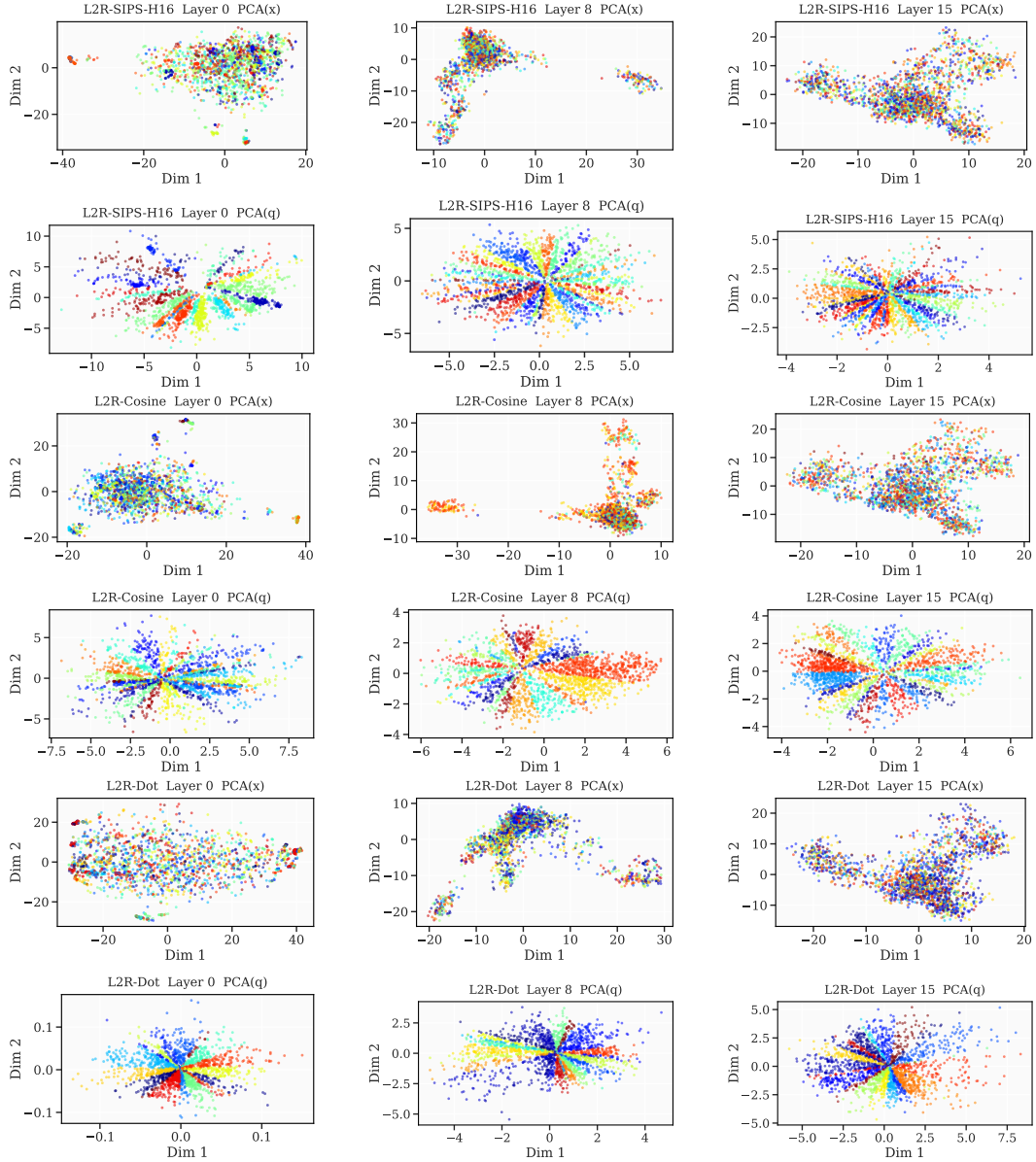


Figure 12: **Routing geometry under L2R.** PCA scatter plots for three representative MoE FFN layers in OLMoE. Points are token representations colored by the top-1 expert. The first row shows backbone representations ( $x$ -space), and the second row shows routing latent queries ( $q$ -space). Compared to  $x$ -space, the  $q$ -space geometry typically exhibits clearer expert-aligned separation and reduced selection ambiguity.

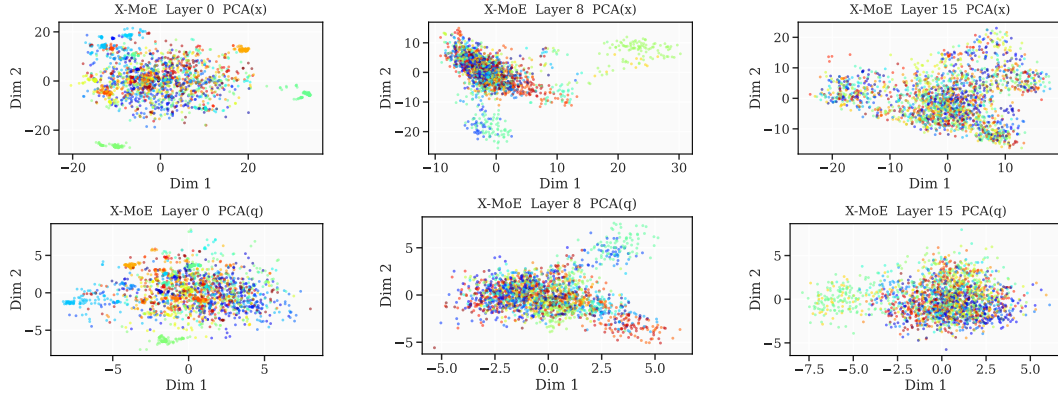


Figure 13: **Routing geometry under the X-MoE router.** PCA projections of token representations at three FFN routing sites (blocks 0/8/15; left to right). Top: backbone activations in the raw representation space  $x$ . Bottom: router features  $q$  used for gating at the corresponding blocks. Each point denotes a token from the same evaluation batch (aggregated across distributed ranks), and colors indicate the selected top-1 expert. The visualization illustrates how token-to-expert partitioning evolves with depth and how separable the routed groups appear in  $x$  versus  $q$ .

### N.3 Expert Usage Heatmaps

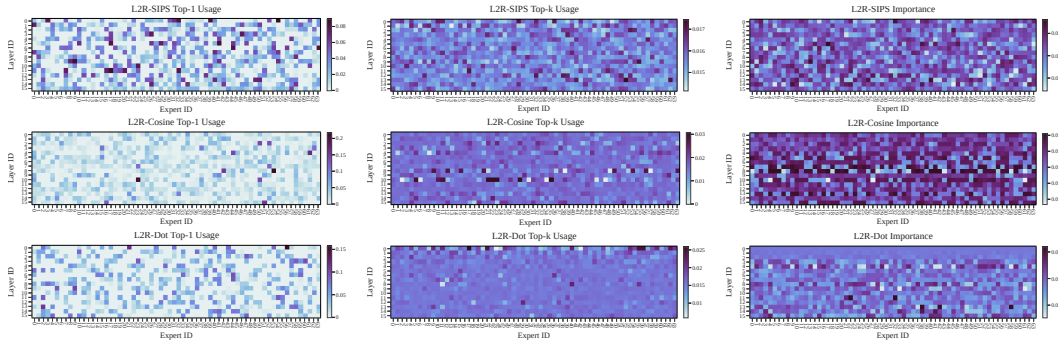


Figure 14: **Expert usage heatmaps for L2R-Cosine, L2R-Dot and L2R-SIPS.** From left to right: Top-1 routing frequency, Top-k routing frequency, and importance-based routing weights. Each row corresponds to a transformer layer and each column corresponds to an expert.

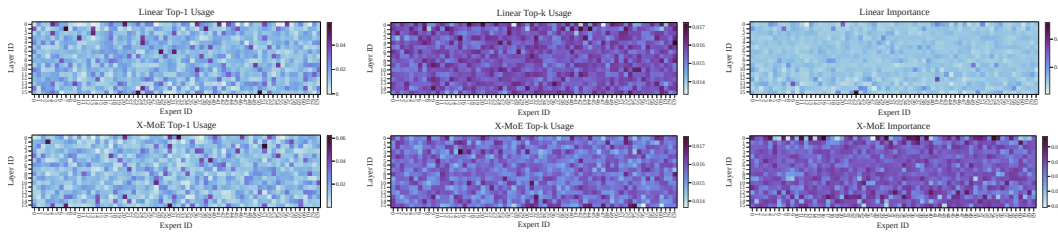


Figure 15: **Expert usage heatmaps for Linear routing and X-MoE.** From left to right: Top-1 routing frequency, Top-k routing frequency, and importance-based routing weights. Each row corresponds to a transformer layer and each column corresponds to an expert.

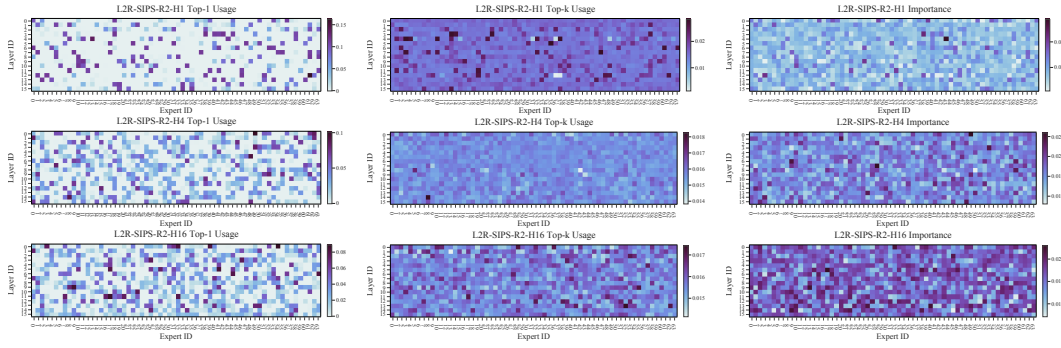


Figure 16: **Expert usage heatmaps under different head settings in L2R-SIPS (Rank=2).** From left to right: Top-1 routing frequency, Top-k routing frequency, and importance-based routing weights. Each row corresponds to a transformer layer, and each column corresponds to an expert.

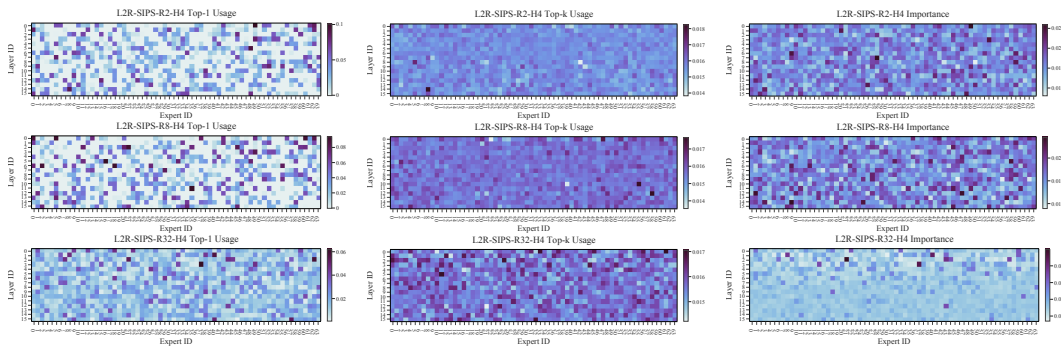


Figure 17: **Expert usage heatmaps under different rank settings in L2R-SIPS (Head=4).** From left to right: Top-1 routing frequency, Top-k routing frequency, and importance-based routing weights. Each row corresponds to a transformer layer, and each column corresponds to an expert.

## NeurIPS Paper Checklist

### 1. Claims

Question: Do the main claims made in the abstract and introduction accurately reflect the paper’s contributions and scope?

Answer: [\[Yes\]](#)

Justification: The abstract and introduction describe L2R as a low-rank and Lipschitz-controlled routing framework, and the main claims are supported by the reported language and vision MoE experiments.

Guidelines:

- The answer [\[N/A\]](#) means that the abstract and introduction do not include the claims made in the paper.
- The abstract and/or introduction should clearly state the claims made, including the contributions made in the paper and important assumptions and limitations. A [\[No\]](#) or [\[N/A\]](#) answer to this question will not be perceived well by the reviewers.
- The claims made should match theoretical and experimental results, and reflect how much the results can be expected to generalize to other settings.
- It is fine to include aspirational goals as motivation as long as it is clear that these goals are not attained by the paper.

### 2. Limitations

Question: Does the paper discuss the limitations of the work performed by the authors?

Answer: [\[Yes\]](#)

Justification: We discuss limitations and future work in Appendix L, including the early-stage OLMoE-based pretraining regime and the need to evaluate longer training, larger MoE configurations, and broader architectures.

Guidelines:

- The answer [N/A] means that the paper has no limitation while the answer [No] means that the paper has limitations, but those are not discussed in the paper.
- The authors are encouraged to create a separate “Limitations” section in their paper.
- The paper should point out any strong assumptions and how robust the results are to violations of these assumptions (e.g., independence assumptions, noiseless settings, model well-specification, asymptotic approximations only holding locally). The authors should reflect on how these assumptions might be violated in practice and what the implications would be.
- The authors should reflect on the scope of the claims made, e.g., if the approach was only tested on a few datasets or with a few runs. In general, empirical results often depend on implicit assumptions, which should be articulated.
- The authors should reflect on the factors that influence the performance of the approach. For example, a facial recognition algorithm may perform poorly when image resolution is low or images are taken in low lighting. Or a speech-to-text system might not be used reliably to provide closed captions for online lectures because it fails to handle technical jargon.
- The authors should discuss the computational efficiency of the proposed algorithms and how they scale with dataset size.
- If applicable, the authors should discuss possible limitations of their approach to address problems of privacy and fairness.
- While the authors might fear that complete honesty about limitations might be used by reviewers as grounds for rejection, a worse outcome might be that reviewers discover limitations that aren’t acknowledged in the paper. The authors should use their best judgment and recognize that individual actions in favor of transparency play an important role in developing norms that preserve the integrity of the community. Reviewers will be specifically instructed to not penalize honesty concerning limitations.

### 3. Theory assumptions and proofs

Question: For each theoretical result, does the paper provide the full set of assumptions and a complete (and correct) proof?

Answer: [Yes]

Justification: The paper defines the SIPS scoring function in the main text and provides the corresponding gradient-sensitivity and Lipschitz-bound analysis in Appendix E.

Guidelines:

- The answer [N/A] means that the paper does not include theoretical results.
- All the theorems, formulas, and proofs in the paper should be numbered and cross-referenced.
- All assumptions should be clearly stated or referenced in the statement of any theorems.
- The proofs can either appear in the main paper or the supplemental material, but if they appear in the supplemental material, the authors are encouraged to provide a short proof sketch to provide intuition.
- Inversely, any informal proof provided in the core of the paper should be complemented by formal proofs provided in appendix or supplemental material.
- Theorems and Lemmas that the proof relies upon should be properly referenced.

### 4. Experimental result reproducibility

Question: Does the paper fully disclose all the information needed to reproduce the main experimental results of the paper to the extent that it affects the main claims and/or conclusions of the paper (regardless of whether the code and data are provided or not)?

Answer: [Yes]

Justification: The paper reports the model settings, routing variants, datasets, objectives, evaluation protocol, and hyperparameters in the main text and appendices.

Guidelines:

- The answer [N/A] means that the paper does not include experiments.
- If the paper includes experiments, a [No] answer to this question will not be perceived well by the reviewers: Making the paper reproducible is important, regardless of whether the code and data are provided or not.
- If the contribution is a dataset and/or model, the authors should describe the steps taken to make their results reproducible or verifiable.
- Depending on the contribution, reproducibility can be accomplished in various ways. For example, if the contribution is a novel architecture, describing the architecture fully might suffice, or if the contribution is a specific model and empirical evaluation, it may be necessary to either make it possible for others to replicate the model with the same dataset, or provide access to the model. In general, releasing code and data is often one good way to accomplish this, but reproducibility can also be provided via detailed instructions for how to replicate the results, access to a hosted model (e.g., in the case of a large language model), releasing of a model checkpoint, or other means that are appropriate to the research performed.
- While NeurIPS does not require releasing code, the conference does require all submissions to provide some reasonable avenue for reproducibility, which may depend on the nature of the contribution. For example
  - (a) If the contribution is primarily a new algorithm, the paper should make it clear how to reproduce that algorithm.
  - (b) If the contribution is primarily a new model architecture, the paper should describe the architecture clearly and fully.
  - (c) If the contribution is a new model (e.g., a large language model), then there should either be a way to access this model for reproducing the results or a way to reproduce the model (e.g., with an open-source dataset or instructions for how to construct the dataset).
  - (d) We recognize that reproducibility may be tricky in some cases, in which case authors are welcome to describe the particular way they provide for reproducibility. In the case of closed-source models, it may be that access to the model is limited in some way (e.g., to registered users), but it should be possible for other researchers to have some path to reproducing or verifying the results.

## 5. Open access to data and code

Question: Does the paper provide open access to the data and code, with sufficient instructions to faithfully reproduce the main experimental results, as described in supplemental material?

Answer: [Yes]

Justification: We provide anonymized code as supplementary material for review, including implementation details and instructions to reproduce the main experiments. A de-anonymized version will be released upon acceptance.

Guidelines:

- The answer [N/A] means that paper does not include experiments requiring code.
- Please see the NeurIPS code and data submission guidelines (<https://neurips.cc/public/guides/CodeSubmissionPolicy>) for more details.
- While we encourage the release of code and data, we understand that this might not be possible, so [No] is an acceptable answer. Papers cannot be rejected simply for not including code, unless this is central to the contribution (e.g., for a new open-source benchmark).
- The instructions should contain the exact command and environment needed to run to reproduce the results. See the NeurIPS code and data submission guidelines (<https://neurips.cc/public/guides/CodeSubmissionPolicy>) for more details.
- The authors should provide instructions on data access and preparation, including how to access the raw data, preprocessed data, intermediate data, and generated data, etc.

- The authors should provide scripts to reproduce all experimental results for the new proposed method and baselines. If only a subset of experiments are reproducible, they should state which ones are omitted from the script and why.
- At submission time, to preserve anonymity, the authors should release anonymized versions (if applicable).
- Providing as much information as possible in supplemental material (appended to the paper) is recommended, but including URLs to data and code is permitted.

## 6. Experimental setting/details

Question: Does the paper specify all the training and test details (e.g., data splits, hyperparameters, how they were chosen, type of optimizer) necessary to understand the results?

Answer: [\[Yes\]](#)

Justification: Training configurations, routing hyperparameters, datasets, evaluation protocols, and implementation details are provided in the main text and Appendix I.

Guidelines:

- The answer [\[Yes\]](#) means that the paper does not include experiments.
- The experimental setting should be presented in the core of the paper to a level of detail that is necessary to appreciate the results and make sense of them.
- The full details can be provided either with the code, in appendix, or as supplemental material.

## 7. Experiment statistical significance

Question: Does the paper report error bars suitably and correctly defined or other appropriate information about the statistical significance of the experiments?

Answer: [\[No\]](#)

Justification: We do not report error bars because full from-scratch MoE training is computationally expensive. Instead, we report consistent trends across multiple routing variants, ablations, and both language and vision settings.

Guidelines:

- The answer [\[N/A\]](#) means that the paper does not include experiments.
- The authors should answer [\[Yes\]](#) if the results are accompanied by error bars, confidence intervals, or statistical significance tests, at least for the experiments that support the main claims of the paper.
- The factors of variability that the error bars are capturing should be clearly stated (for example, train/test split, initialization, random drawing of some parameter, or overall run with given experimental conditions).
- The method for calculating the error bars should be explained (closed form formula, call to a library function, bootstrap, etc.)
- The assumptions made should be given (e.g., Normally distributed errors).
- It should be clear whether the error bar is the standard deviation or the standard error of the mean.
- It is OK to report 1-sigma error bars, but one should state it. The authors should preferably report a 2-sigma error bar than state that they have a 96% CI, if the hypothesis of Normality of errors is not verified.
- For asymmetric distributions, the authors should be careful not to show in tables or figures symmetric error bars that would yield results that are out of range (e.g., negative error rates).
- If error bars are reported in tables or plots, the authors should explain in the text how they were calculated and reference the corresponding figures or tables in the text.

## 8. Experiments compute resources

Question: For each experiment, does the paper provide sufficient information on the computer resources (type of compute workers, memory, time of execution) needed to reproduce the experiments?

Question: For each experiment, does the paper provide sufficient information on the computer resources (type of compute workers, memory, time of execution) needed to reproduce the experiments?

Answer: [Yes]

Justification: The paper reports the GPU types used for the language and vision experiments, and Appendix F provides efficiency analysis and timing measurements. We do not report exhaustive memory traces for every run, but the provided compute and timing information is sufficient to understand the resource requirements of the main experiments.

Guidelines:

- The answer [N/A] means that the paper does not include experiments.
- The paper should indicate the type of compute workers CPU or GPU, internal cluster, or cloud provider, including relevant memory and storage.
- The paper should provide the amount of compute required for each of the individual experimental runs as well as estimate the total compute.
- The paper should disclose whether the full research project required more compute than the experiments reported in the paper (e.g., preliminary or failed experiments that didn't make it into the paper).

## 9. Code of ethics

Question: Does the research conducted in the paper conform, in every respect, with the NeurIPS Code of Ethics <https://neurips.cc/public/EthicsGuidelines?>

Answer: [Yes]

Justification: The work studies MoE routing mechanisms using existing research datasets and does not involve human subjects, private data, or deceptive data collection.

Guidelines:

- The answer [N/A] means that the authors have not reviewed the NeurIPS Code of Ethics.
- If the authors answer [No], they should explain the special circumstances that require a deviation from the Code of Ethics.
- The authors should make sure to preserve anonymity (e.g., if there is a special consideration due to laws or regulations in their jurisdiction).

## 10. Broader impacts

Question: Does the paper discuss both potential positive societal impacts and negative societal impacts of the work performed?

Answer: [Yes]

Justification: The paper discusses broader impacts in Appendix M. In this study, we propose a new routing framework for Mixture-of-Experts models, which may yield positive impacts, including improving conditional computation efficiency, reducing computational resource requirements, and potentially decreasing energy consumption associated with large-scale training and inference.

Guidelines:

- The answer [N/A] means that there is no societal impact of the work performed.
- If the authors answer [N/A] or [No], they should explain why their work has no societal impact or why the paper does not address societal impact.
- Examples of negative societal impacts include potential malicious or unintended uses (e.g., disinformation, generating fake profiles, surveillance), fairness considerations (e.g., deployment of technologies that could make decisions that unfairly impact specific groups), privacy considerations, and security considerations.
- The conference expects that many papers will be foundational research and not tied to particular applications, let alone deployments. However, if there is a direct path to any negative applications, the authors should point it out. For example, it is legitimate to point out that an improvement in the quality of generative models could be used to generate Deepfakes for disinformation. On the other hand, it is not needed to point out

that a generic algorithm for optimizing neural networks could enable people to train models that generate Deepfakes faster.

- The authors should consider possible harms that could arise when the technology is being used as intended and functioning correctly, harms that could arise when the technology is being used as intended but gives incorrect results, and harms following from (intentional or unintentional) misuse of the technology.
- If there are negative societal impacts, the authors could also discuss possible mitigation strategies (e.g., gated release of models, providing defenses in addition to attacks, mechanisms for monitoring misuse, mechanisms to monitor how a system learns from feedback over time, improving the efficiency and accessibility of ML).

## 11. Safeguards

Question: Does the paper describe safeguards that have been put in place for responsible release of data or models that have a high risk for misuse (e.g., pre-trained language models, image generators, or scraped datasets)?

Answer: [N/A]

Justification: The paper does not release a new pretrained model, image generator, or scraped dataset with high misuse risk.

Guidelines:

- The answer [N/A] means that the paper poses no such risks.
- Released models that have a high risk for misuse or dual-use should be released with necessary safeguards to allow for controlled use of the model, for example by requiring that users adhere to usage guidelines or restrictions to access the model or implementing safety filters.
- Datasets that have been scraped from the Internet could pose safety risks. The authors should describe how they avoided releasing unsafe images.
- We recognize that providing effective safeguards is challenging, and many papers do not require this, but we encourage authors to take this into account and make a best faith effort.

## 12. Licenses for existing assets

Question: Are the creators or original owners of assets (e.g., code, data, models), used in the paper, properly credited and are the license and terms of use explicitly mentioned and properly respected?

Answer: [No]

Justification: The paper cites the original sources of the models, datasets, and benchmarks used in the experiments, but does not explicitly list the licenses and terms of use for each asset.

Guidelines:

- The answer [N/A] means that the paper does not use existing assets.
- The authors should cite the original paper that produced the code package or dataset.
- The authors should state which version of the asset is used and, if possible, include a URL.
- The name of the license (e.g., CC-BY 4.0) should be included for each asset.
- For scraped data from a particular source (e.g., website), the copyright and terms of service of that source should be provided.
- If assets are released, the license, copyright information, and terms of use in the package should be provided. For popular datasets, [paperswithcode.com/datasets](https://paperswithcode.com/datasets) has curated licenses for some datasets. Their licensing guide can help determine the license of a dataset.
- For existing datasets that are re-packaged, both the original license and the license of the derived asset (if it has changed) should be provided.
- If this information is not available online, the authors are encouraged to reach out to the asset's creators.

## 13. New assets

Question: Are new assets introduced in the paper well documented and is the documentation provided alongside the assets?

Answer: [N/A]

Justification: The paper does not introduce a new dataset or pretrained model asset. The planned release is code for reproducing the proposed routing method.

Guidelines:

- The answer [N/A] means that the paper does not release new assets.
- Researchers should communicate the details of the dataset/code/model as part of their submissions via structured templates. This includes details about training, license, limitations, etc.
- The paper should discuss whether and how consent was obtained from people whose asset is used.
- At submission time, remember to anonymize your assets (if applicable). You can either create an anonymized URL or include an anonymized zip file.

#### 14. Crowdsourcing and research with human subjects

Question: For crowdsourcing experiments and research with human subjects, does the paper include the full text of instructions given to participants and screenshots, if applicable, as well as details about compensation (if any)?

Answer: [N/A]

Justification: The paper does not involve crowdsourcing or research with human subjects.

Guidelines:

- The answer [N/A] means that the paper does not involve crowdsourcing nor research with human subjects.
- Including this information in the supplemental material is fine, but if the main contribution of the paper involves human subjects, then as much detail as possible should be included in the main paper.
- According to the NeurIPS Code of Ethics, workers involved in data collection, curation, or other labor should be paid at least the minimum wage in the country of the data collector.

#### 15. Institutional review board (IRB) approvals or equivalent for research with human subjects

Question: Does the paper describe potential risks incurred by study participants, whether such risks were disclosed to the subjects, and whether Institutional Review Board (IRB) approvals (or an equivalent approval/review based on the requirements of your country or institution) were obtained?

Answer: [N/A]

Justification: The paper does not involve human subjects, so IRB approval is not applicable.

Guidelines:

- The answer [N/A] means that the paper does not involve crowdsourcing nor research with human subjects.
- Depending on the country in which research is conducted, IRB approval (or equivalent) may be required for any human subjects research. If you obtained IRB approval, you should clearly state this in the paper.
- We recognize that the procedures for this may vary significantly between institutions and locations, and we expect authors to adhere to the NeurIPS Code of Ethics and the guidelines for their institution.
- For initial submissions, do not include any information that would break anonymity (if applicable), such as the institution conducting the review.

#### 16. Declaration of LLM usage

Question: Does the paper describe the usage of LLMs if it is an important, original, or non-standard component of the core methods in this research? Note that if the LLM is used only for writing, editing, or formatting purposes and does *not* impact the core methodology, scientific rigor, or originality of the research, declaration is not required.

Answer: [N/A]

Justification: The core method does not use LLMs as an important, original, or non-standard component. MoE language models are used only as experimental architectures for evaluating the proposed routing method.

Guidelines:

- The answer [N/A] means that the core method development in this research does not involve LLMs as any important, original, or non-standard components.
- Please refer to our LLM policy in the NeurIPS handbook for what should or should not be described.